Instabilities in anisotropic plasmas

P.L. Sulem
UNS, CNRS, Observatoire de la Côte d'Azur, Nice

ECOLE DE PHYSIQUE des HOUCHES
The future of plasma astrophysics: combining experiments, observations, simulations, and theory (February 25-March 8, 2013)

Anisotropic plasmas refer to situations where the velocity distribution functions of the various particle species are non isotropic (in particular non Maxwellian).

Such a regime requires Coulomb collisions to be sufficiently weak.

Many astrophysical plasmas are magnetized and weakly or even almost non collisional.

Characterized by:

Collision frequency << cyclotron frequency
Larmor radius << mean free path

Examples include

- Galaxy cluster plasmas *Schekochihin et al. ApJ **629**, 139 (2005)*
- Solar wind *Marsch , Space Sc. Rev. **172**, 22, (2012)*
- Planet magnetospheres *Blanc et al. Space Sci. Rev. **116**, 227 (2005)*
- . . .

In situ observations in the solar wind

Velocity distribution functions exhibit large departures from isotropic (Maxwellian) distribution functions:

- Different **parallel** and **perpendicular temperatures** with respect to the ambient magnetic field.

- The proton distribution function often exhibit a **core** and a magnetic field-aligned **beam** with

- a number density of the order of tenths of the core density
- the beam/core relative velocity of the order of the local Alfvén velocity

*(Marsch et al., JGR **87**, 35, 1982*).

In magnetized collisionless (or weakly collisional) plasmas, the velocity distribution function of each particle species is not Maxwellian.

Anisotropy of the proton distribution function of slow (left), intermediate speed (middle) and fast solar wind at increasing distances from the sun.

----- : direction of the magnetic field

Marsch , Space Sc. Rev. ***172****, 22, 2012*

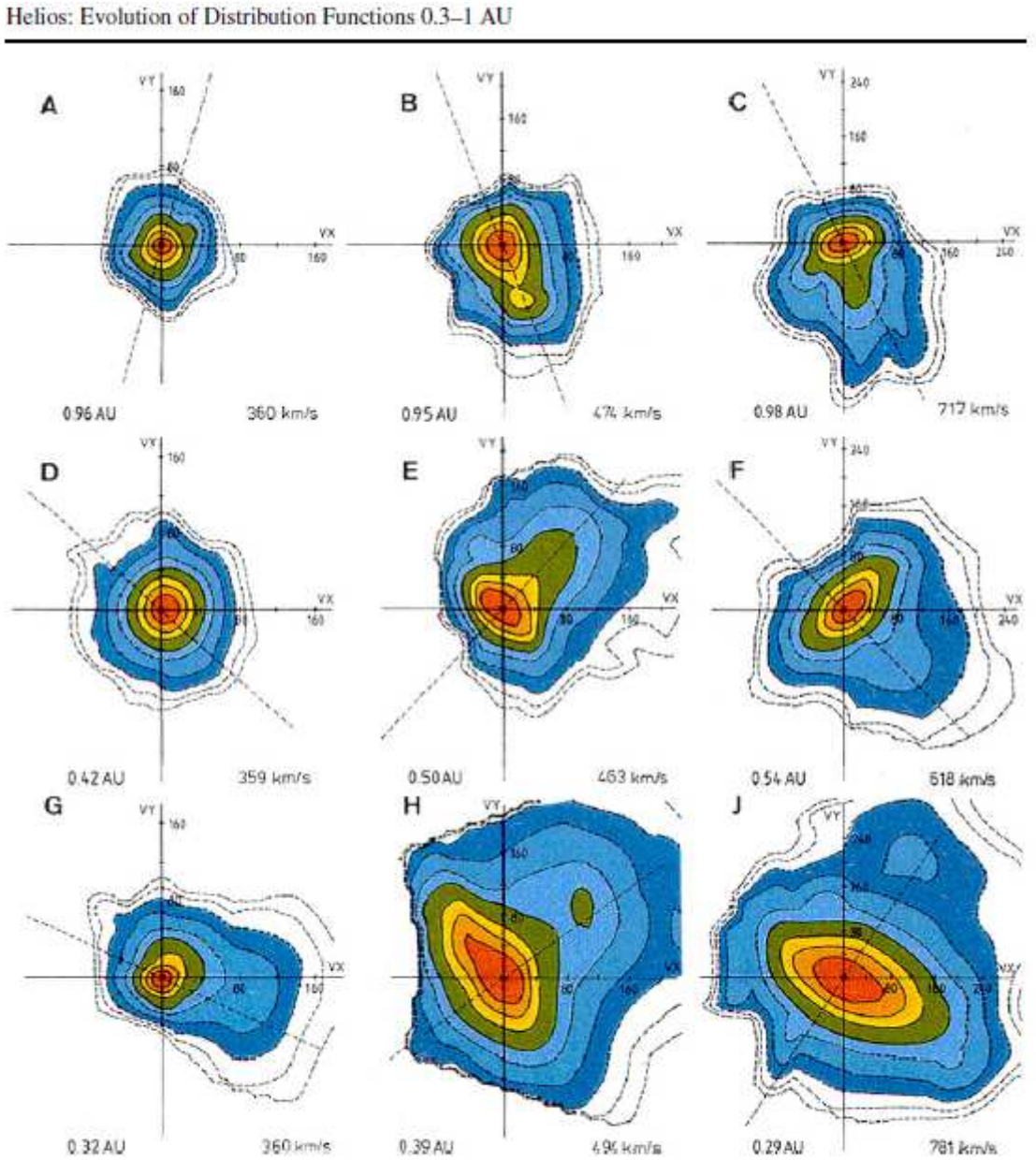

Fig. 1 Proton velocity distribution functions for three types of solar wind: Slow (*left column*), intermediate-speed (*middle*), and fast (*right*). The heliocentric distance decreases from top to bottom as indicated in the respective frames. Increasingly strong deviations from a Maxwellian occur at smaller distances from the Sun, with proton beams along the field (*dashed lines*) and large anisotropies perpendicular to the field in the core

In this talk,

I concentrate on the effect of **temperature anisotropy**
(assuming an equilibrium bi-Maxwellian velocity distribution function)
and will not address the effect of beams.

I concentrate on instabilities that require the **presence of an ambient magnetic field**
and will thus not discuss instabilities such as the *Weibel instability* (driven by an anisotropic electron distribution in the presence of immobile neutralizing ions; enhances initial magnetic fluctuations).

Pressure tensor of a magnetized collisionless plasmas

The **pressure** of each particle species *r* (of mass m_r)

$$\mathbf{p}_r(\vec{x},t) = m_r \int (\vec{v}-\vec{u}_r) \otimes (\vec{v}-\vec{u}_r)\, f_r(\vec{x},\vec{v},t)\, d\vec{v}$$

is a **full tensor**.

Here, $\vec{u}_r(\vec{x},t) = \dfrac{1}{n_r}\int \vec{v} f_r(\vec{x},\vec{v},t) d\vec{v}$ is the corresponding **hydrodynamic velocity**.

$n_r(\vec{x},t) = \int f_r(\vec{x},\vec{v},t) d\vec{v}$ is the number density of particles of species *r*

Pressure anisotropy is a source of free energy *(energy that can be transformed into work).*
The system will tend to relax or to reduce this anisotropy via collisions or, if they are too weak to act efficiently, by developing **instabilities** which push the system towards equilibrium.

It is often convenient to separate the **gyrotropic** part of the pressure tensor
(characterized by the *perpendicular* and *parallel pressures*)
from the **non-gyrotropic** part (also called **finite Larmor radius or FLR corrections**)

$$\mathbf{p}_r = p_{\perp r}\mathbf{n} + p_{\parallel r}\boldsymbol{\tau} + \boldsymbol{\Pi}_r$$

$$\mathbf{n} = \mathbf{I} - \hat{b}\otimes\hat{b} \qquad \boldsymbol{\tau} = \hat{b}\otimes\hat{b} \qquad \hat{b} = \vec{B}/|\vec{B}|$$

At scales large compared with the Larmor radius, the non-gyrotropic part is subdominant.

From the perpendicular and parallel pressures ,

$$p_{\perp r} = \frac{1}{2}\,\mathbf{p}_r : \mathbf{n} \qquad p_{\parallel r} = \mathbf{p}_r : \boldsymbol{\tau}$$

one defines the *perpendicular* and *parallel temperatures*

$$T_{\perp r} = \frac{p_{\perp r}}{n_r} \qquad T_{\parallel r} = \frac{p_{\parallel r}}{n_r}$$

n_r : number density

The perpendicular and parallel pressures of each species *r* obey equations derived from the Vlasov equation

$$\partial_t p_{\perp r} + \nabla \cdot (\vec{u}_r\, p_{\perp r}) + p_{\perp r} \nabla \cdot \vec{u}_r - p_{\perp r}\, \widehat{b} \cdot \nabla \vec{u}_r \cdot \widehat{b}$$
$$+\frac{1}{2}\Big(\mathrm{tr}\, \nabla \cdot \mathbf{q}_r - \widehat{b} \cdot (\nabla \cdot \mathbf{q}_r) \cdot \widehat{b}\Big)$$
$$+\frac{1}{2}\Big(\mathrm{tr}\, (\mathbf{\Pi}_r \cdot \nabla \vec{u}_r)^S - (\mathbf{\Pi}_r \cdot \nabla \vec{u}_r)^S : \boldsymbol{\tau} + \mathbf{\Pi}_r : \frac{d\boldsymbol{\tau}}{dt}\Big) = 0$$

$$\partial_t p_{\parallel r} + \nabla \cdot (\vec{u}_r\, p_{\parallel r}) + 2 p_{\parallel r}\, \widehat{b} \cdot \nabla \vec{u}_r \cdot \widehat{b} + \widehat{b} \cdot (\nabla \cdot \mathbf{q}_r) \cdot \widehat{b}$$
$$+(\mathbf{\Pi}_r \cdot \nabla \vec{u}_r)^S : \boldsymbol{\tau} - \mathbf{\Pi}_r : \frac{d\boldsymbol{\tau}}{dt} = 0,$$

$\mathbf{q}_r$: heat flux tensor

In the absence of collisions, pressure and temperature anisotropies can develop even if the plasma is initially isotropic.

Example: Expanding plasma (solar wind)

Simple model:

- Consider **the dynamics at scales large compared to the ion Larmor radius** (**FLR contributions** and **Hall term negligible**)
- **Neglect heat fluxes**

Combining the equations for the perpendicular and parallel **ion pressures** with the density and induction equations (where Hall effect is neglected),

$$\frac{d}{dt}\left(\frac{p_\perp}{\rho B}\right) = 0$$
$$\frac{d}{dt}\left(\frac{p_\parallel B^2}{\rho^3}\right) = 0$$

One can impose the equations of state

$$\begin{cases} \dfrac{p_\perp}{\rho B} = \text{cst} \\ \dfrac{p_\parallel B^2}{\rho^3} = \text{cst} \end{cases}$$

Double adiabatic approximation
(Chew,Goldberg & Low, 1956)

Double-adiabatic (or CGL) approximation

$$\frac{p_\perp}{\rho B} = \mathrm{cst}$$

$$\frac{p_\parallel B^2}{\rho^3} = \mathrm{cst}$$

For a spherical expansion, in the presence of a strictly radial magnetic field and a constant solar wind velocity where

$$B \propto \frac{1}{R^2} \qquad \rho \propto \frac{1}{R^2}$$

one gets

$$T_\perp \propto \frac{1}{R^2} \qquad T_\parallel = cst$$

and

$$\beta_\parallel \propto \frac{p_\parallel}{B^2} \propto R^2 \propto \frac{T_\parallel}{T_\perp}$$

Fig. 3 Evolution of proton temperature anisotropy in the solar wind from Helios observations (Matteini et al. 2007): Contours of the observed frequency of $\beta_{p\parallel}$, $T_{p\perp}/T_{p\parallel}$ at (*dashed*) 0.3 AU and (*solid*) 1 AU. *Dotted line* displays the CGL predictions for a strictly radial magnetic field $T_{p\perp}/T_{p\parallel} \propto 1/\beta_{p\parallel}$. *Dash-dotted line* shows the empirical anti-correlation inferred by data between 0.3 and 1 AU (Marsch et al. 2004)

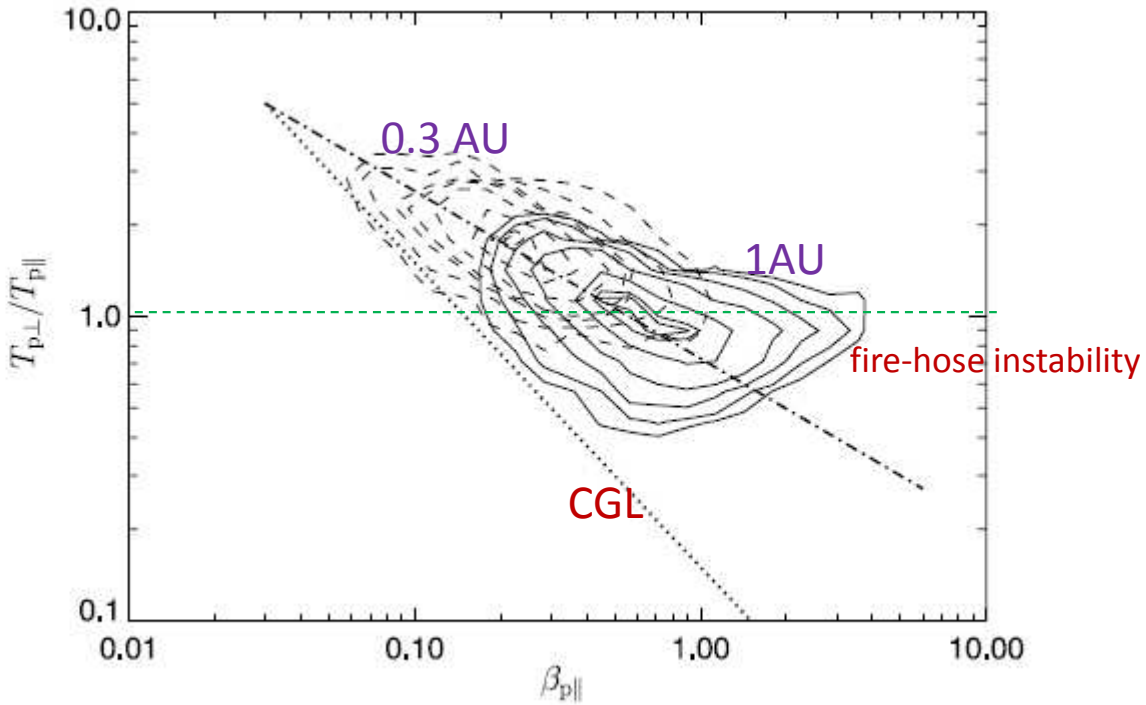

Matteini et al., Space Sci. Rev. ***172****, 373, 2011*

The observed anticorrelation $\beta_{p\parallel}, T_{p\perp}/T_{p\parallel}$ departs from the CGL prediction.

Suggests **perpendicular heating** by turbulence (not addressed here).
Parallel cooling may also be required *(Hellinger et al. JGR, in press).*

For $\beta_{p\parallel} > 1$, data show departure from the empirical correlation observed at lower $\beta_{p\parallel}$.
Related to the fact that for $\beta_{p\parallel} > 1$, anisotropic plasmas with $T_{p\parallel} > T_{p\perp}$ can develop a fire-hose instability.

Statistical study of temperature anisotropies in the slow solar wind

Solar wind expansion and turbulence generate temperature anisotropy
This anisotropy is limited by micro-instabilities: mirror and oblique firehose instabilities.

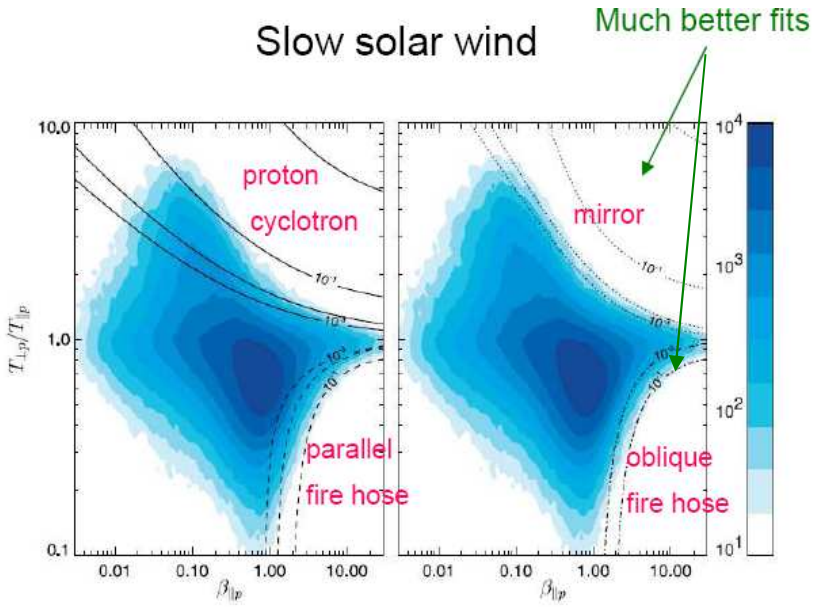

Figure 1. A color scale plot of the relative frequency of ($\beta_{\parallel p}$, $T_{\perp p}/T_{\parallel p}$) in the WIND/SWE data (1995–2001) for the solar wind with $v_{sw} \leq 600$ km/s [cf. *Kasper et al.*, 2002, Figure 2]. The (logarithmic) color scale is show on the right. The over plotted curves show the contours of the maximum growth rate (in units of ω_{cp}) in the corresponding bi-Maxwellian plasma (left) for the proton cyclotron instability (solid curves) and the parallel fire hose (dashed curves) and (right) for the mirror instability (dotted curves) and the oblique fire hose (dash-dotted curves).

Hellinger et al. ,GRL **33**, L09101 (2006)

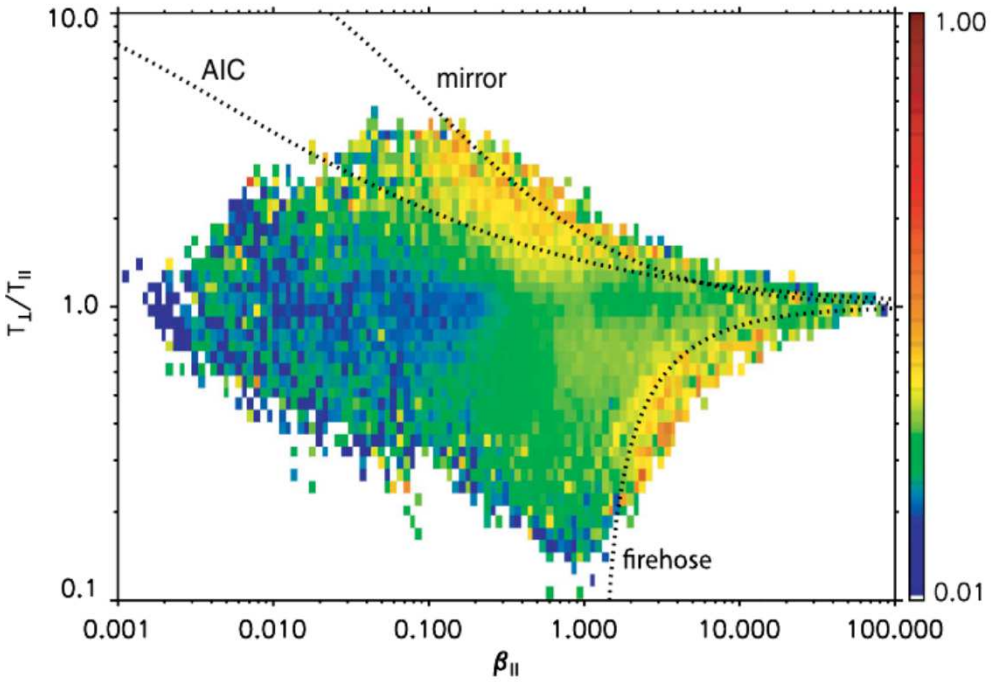

Bale et al. PRL 103, 21101 (2009)

color: magnitude of δB; enhanced δB also corresponds to enhanced proton heating.

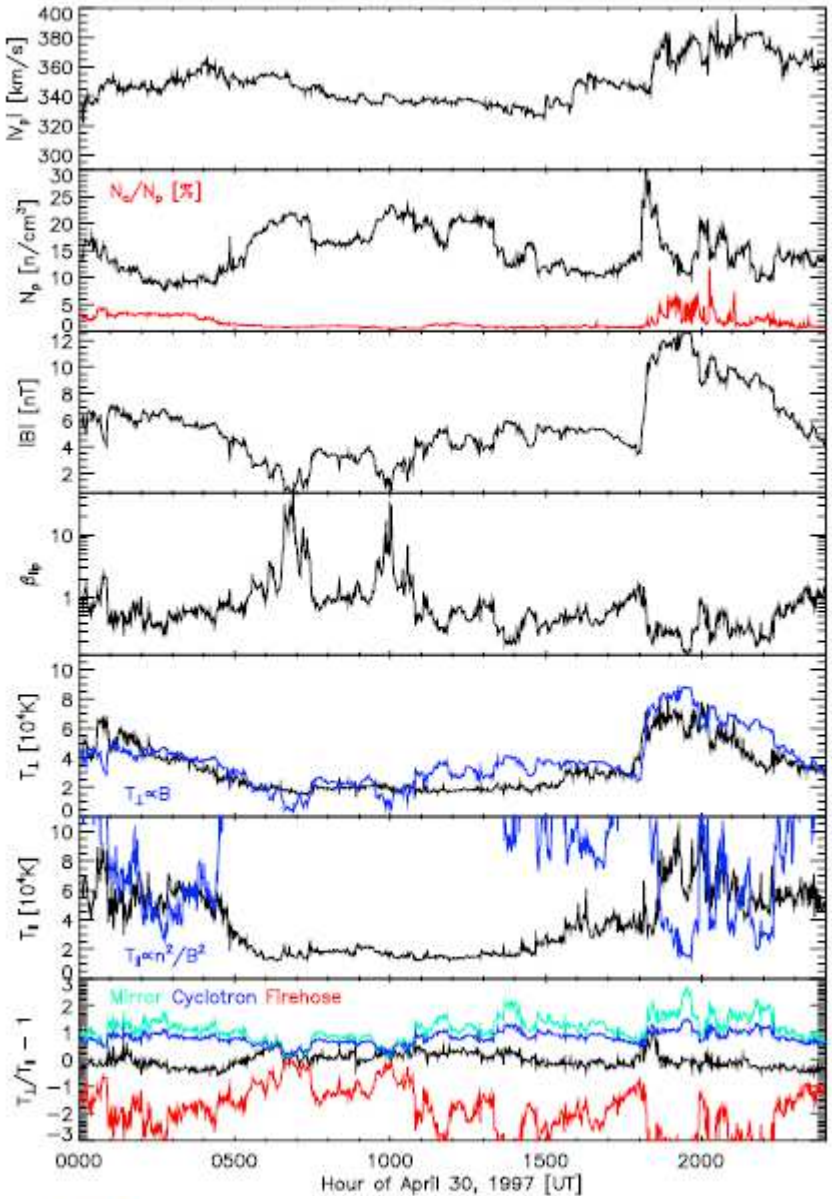

FIGURE 1. Solar wind observations by the Wind spacecraft on April 30, 1997. The alpha particle abundance is very low and may be neglected. Note that the predicted value of $T_{\|}$ is very high and off the scale of the plot for 0500-1500 UT.

Kasper et al., Solar Wind 10, 2003

Parallel temperature far from bi-adiabatic prediction

Temperature anisotropy constrained to stay within the strip defined by micro-instabilities.

Plasmas instabilities

- macroscopic (configurational) instabilities: can be described by macroscopic equations in configuration space.

- microinstabilities instabilities : depend on the actual shape of the distribution function.

For a detailed study of the microinstabilities based on a fully kinetic description:

- S.P. Gary, *Theory of Space Plasma Microinstabilities* , Cambridge Univ. Press, 1993 (reprinted 2005).
- Schlickeiser, Lazar & Skoda, *Phys. Plasmas* **18**, 012103, 2011 (and references therein)
- R.A. Treumann & W.B. Baumjohann, *Advanced Space Plasma Physics,* Imperial College Press, 1997.

Instabilities do not arise without free energy.

Free energy may come from the magnetic configuration (stored e.g. in the Harris current sheet) , **anisotropic plasma pressure**, streaming of plasma particles with respect to each other, etc.

Main microinstabilities due to anisotropic ion pressure in a magnetized plasma

$T_\perp < T_\parallel$

- Parallel (or whistler) fire-hose instability — whistler waves
- Oblique (or Alfvén) fire-hose instability — oblique (or kinetic) Alfvén waves

$T_\perp > T_\parallel$

- Mirror instability — mirror modes
- Proton cyclotron instability — ion-cyclotron waves

The presence of a small density of helium ions can significantly reduce the proton cyclotron instability growth rate, making the mirror instability dominant *(Price et al., JGR, **91**, 101, 1986).*

Analogous instabilities can be driven by anisotropic electron pressure

*(Gary & Karimabadi, JGR **111**, A11224, 2006; Steverak et al. JGR **113**, A03103, 2008)*

The parallel (or whistler) fire-hose instability

This instability can be correctly analyzed within a **fluid description** *(outside ion-cyclotron resonance).*

Consider a plasma at equilibrium, with anisotropic pressure, subject to an ambient **magnetic field in the z direction**. We first consider the large-scale dynamics.

Linearize the induction equation (neglecting Hall effect)

$$\partial_t \vec{B}' = \nabla \times (\vec{u} \times B_0 \hat{z})$$

$$\vec{B} = B_0 \hat{z} + \vec{B}'$$

Define the *displacement vector* $\vec{u} = \partial_t \vec{\xi}$

$$\Longrightarrow \quad \vec{B}' = \nabla \times (\vec{\xi} \times B_0 \hat{z})$$

For a mode with wavevector $\vec{k} = (k_x, 0, k_z)$

$$\vec{B}' = B_0 (i k_z \xi_x \, , i k_z \xi_y \, , -i k_x \xi_x)$$

$$\vec{B} = B_0 (i k_z \xi_x \, , i k_z \xi_y \, , 1 - i k_x \xi_x)$$

$$\hat{b} = \frac{\vec{B}}{|\vec{B}|} = (i k_z \xi_x \, , i k_z \xi_y \, , 1)$$

Pressure fluctuations:

$$\mathbf{p}' = p'_{\perp}\mathbf{I} + (p'_{\parallel} - p'_{\perp})\widehat{z}\otimes\widehat{z} + (p_{0\parallel} - p_{0\perp})(\widehat{b}'\otimes\widehat{z} + \widehat{z}\otimes\widehat{b}')$$

where $\widehat{b}' = \widehat{b} - \widehat{z} = ik_z\vec{\xi}_{\perp}$

Thus

$$\begin{aligned}\nabla\cdot\mathbf{p}' &= [ik_x p'_{\perp} - (p_{0\parallel} - p_{0\perp})k_z^2\xi_x]\widehat{x} \\ &\quad -(p_{0\parallel} - p_{0\perp})k_z^2\xi_y\widehat{y} \\ &\quad +[ik_z p'_{\parallel} - (p_{0\parallel} - p_{0\perp})k_x k_z\xi_x]\widehat{z}\end{aligned}$$

Lorentz force:

$$\frac{1}{4\pi}(\nabla\times\vec{B}')\times B_0\widehat{z} = -\frac{B_0^2}{4\pi}[(k_x^2 + k_z^2)\xi_x\widehat{x} + k_z^2\xi_y\widehat{y}$$

Substituting in the **linearized velocity equation**

$$\rho_0\partial_t\vec{u} + \nabla\cdot\mathbf{p}' = \frac{1}{4\pi}(\nabla\times\vec{B}')\times B_0\widehat{z}$$

gives

$$\begin{cases} -\rho_0\omega^2\xi_x + ik_x p'_{\perp} - (p_{0\parallel} - p_{0\perp})k_z^2\xi_x + \dfrac{B_0}{4\pi}(k_x^2 + k_z^2)\xi_x = 0 \\ -\rho_0\omega^2\xi_y - (p_{0\parallel} - p_{0\perp})k_z^2\xi_y + \dfrac{B_0}{4\pi}k_z^2\xi_y = 0 \\ -\rho_0\omega^2\xi_z + ik_z p'_{\parallel} - (p_{0\parallel} - p_{0\perp})k_x k_z\xi_x = 0 \end{cases}$$

When assuming purely longitudinal perturbations ($k_x=0$),

$$\begin{cases} -\rho_0\omega^2\xi_x + ik_x p'_\perp - (p_{0\parallel} - p_{0\perp})k_z^2\xi_x + \dfrac{B_0}{4\pi}(k_x^2 + k_z^2)\xi_x = 0 \\ -\rho_0\omega^2\xi_y - (p_{0\parallel} - p_{0\perp})k_z^2\xi_y + \dfrac{B_0}{4\pi}k_z^2\xi_y = 0 \\ -\rho_0\omega^2\xi_z + ik_z p'_\parallel - (p_{0\parallel} - p_{0\perp})k_x k_z \xi_x = 0 \end{cases}$$

- the dynamics of the transverse field components decouples
- **it is not necessary to specify the pressure field**: no kinetic physics is required.

$$-\rho\omega^2 = \left[(p_{0\parallel} - p_{0\perp}) - \frac{B_0^2}{4\pi}\right] k_z^2$$

The **instability condition** can be written in several forms :

$$p_{0\parallel} > p_{0\perp} + \frac{B_0^2}{4\pi}$$

$$\frac{T_{0\parallel}}{T_{0\perp}} - 1 > \frac{2}{\beta_\perp}$$

$$\frac{T_{0\perp}}{T_{0\parallel}} - 1 + \frac{2}{\beta_\parallel} < 0$$

$$\beta_\parallel - \beta_\perp > 2$$

$$\beta_\parallel = \frac{8\pi p_{0\parallel}}{B_0^2} \qquad \beta_\perp = \frac{8\pi p_{0\perp}}{B_0^2}$$

Growth rate
(at the largest scales)

$$\gamma = k_z \frac{v_A}{\sqrt{2}} (\beta_\parallel - \beta_\perp - 2)^{\frac{1}{2}}$$

$$v_A^2 = \frac{B_0^2}{4\pi\rho_0}$$

Alfvénic eigenmode:

$$\frac{\vec{B}'}{B_0} = ik_z(\xi_x, \xi_y, 0) = -\frac{k_z}{\omega}(u_x, u_y, 0)$$

The instability survives in weakly oblique directions in a cone whose angle increases with beta, but is maximal in the parallel direction
(*Gary et al. , JGR, **103**, 14574, 1998* where a kinetic approach is presented)

Physical interpretation of the parallel fire-hose instability

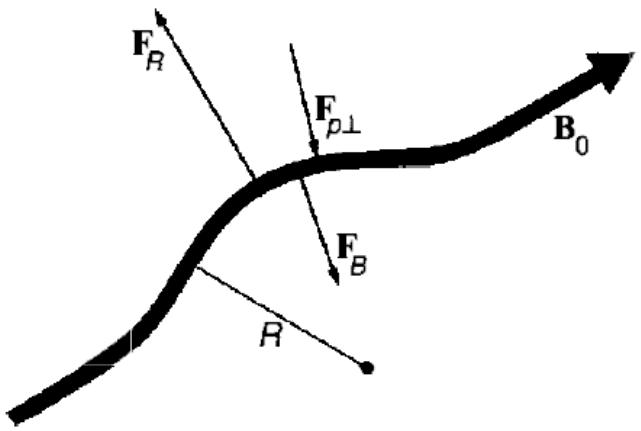

Fig. 3.7. Mechanism of the firehose instability.

(from Treumann & Baumjohann Advanced Space Plasma Physics, 1997)

Consider a magnetic flux tube.

The plasma flows along the magnetic field with the typical velocity $v_{th\|}$.

Whenever a flux tube is slightly bent, the plasma exerts a **centrifugal force**

$$F_R = m_i n_0 v_{th\|}^2 / R$$

Two forces resist to this centrifugal force:

The **thermal pressure force** in the plane perpendicular to the flux tube

$$F_{p\perp} = p_\perp / R$$

The **magnetic stresses of the flux tube**

$$F_B = B_0^2/(4\pi R)$$

Instability sets in if $F_R > F_{p\perp} + F_B$, i.e. $\dfrac{m_i n_0 v_{th\|}^2}{R} > \dfrac{p_\perp}{R} + \dfrac{B_0^2}{4\pi R}$ or $p_\| > p_\perp + \dfrac{B_0^2}{4\pi}$

Growth rate

$$\gamma = k_z \frac{v_A}{\sqrt{2}} (\beta_{\parallel} - \beta_{\perp} - 2)^{\frac{1}{2}}$$

Within this (large-scale) description, the instability growth rate increases linearly with the perturbation wavenumber.

The instability is in fact arrested at small scales by the Hall term and the pressure FLR corrections.

These effects are to be retained for the initial value problem to be well-posed.

Hall term *(neglect contribution of electron pressure gradient)*

$$\partial_t \vec{B} = -c\nabla \times \vec{E} \qquad \vec{E} + \frac{1}{c}\vec{u}_e \times \vec{B} = 0$$

$$\vec{u}_e = \vec{u} - \frac{\vec{j}}{en} \qquad \vec{j} = \frac{c}{4\pi}\nabla \times \vec{B} \qquad (\vec{u} = \vec{u}_i\,)$$

$$\vec{E} = -\left(\vec{u} - \frac{c}{en}\frac{\nabla \times \vec{B}}{4\pi}\right) \times \frac{\vec{B}}{c}$$

$$\partial_t \vec{B} = \nabla \times \left(\vec{u} \times \vec{B} - \frac{1}{\Omega_i}\frac{B_0}{4\pi\rho}(\nabla \times \vec{B}) \times \vec{B}\right) \qquad \Omega_i = \frac{eB_0}{m_i c}$$

Ion gyrofrequency

When linearized,

$$-i\omega \vec{B}'_\perp = B_0 i k_z \vec{u}_\perp + \frac{v_A^2}{\Omega_i} k_z^2 (\hat{z} \times \vec{B}'_\perp)$$

Large-scale pressure FLR corrections (after linearization)

$$\Pi_{xx} = -\Pi_{yy} = -\frac{p_{0\perp}}{2\Omega_i}(\partial_y u_x + \partial_x u_y),$$

$$\Pi_{xy} = \Pi_{yx} = -\frac{p_{0\perp}}{2\Omega_i}(\partial_y u_y - \partial_x u_x),$$

$$\Pi_{yz} = \Pi_{zy} = \frac{1}{\Omega_i}\left[2p_{0\parallel}\partial_z u_x + p_{0\perp}(\partial_x u_z - \partial_z u_x) + \partial_x q_\perp\right],$$

$$\Pi_{xz} = \Pi_{zx} = -\frac{1}{\Omega_i}\left[2p_{0\parallel}\partial_z u_y + p_{0\perp}(\partial_y u_z - \partial_z u_y) + \partial_y q_\perp\right],$$

$$\Pi_{zz} = 0$$

Gyrotropic pressure fluctuations (linearized form)

$$\mathbf{p}'_{\text{gyro}} = p'_\perp \mathbf{I} + (p'_\parallel - p'_\perp)\hat{z}\otimes\hat{z} + (p_{0\parallel} - p_{0\perp})(\hat{b}'\otimes\hat{z} + \hat{z}\otimes\hat{b}')$$

$$= p'_\perp(\hat{x}\otimes\hat{x} + \hat{y}\otimes\hat{y}) + p'_\parallel\hat{z}\otimes\hat{z} + (p_{0\parallel} - p_{0\perp})\left(\frac{\vec{B}'}{B_0}\otimes\hat{z} + \hat{z}\otimes\frac{\vec{B}'}{B_0}\right)$$

For parallel perturbations $\nabla = \hat{z}\,\partial_z$

So $(\nabla\cdot\mathbf{p}')_\perp = 0$

Lorentz force

$$\begin{aligned}\frac{1}{4\pi}(\nabla\times\vec{B}')\times B_0\widehat{z} &= -\frac{B_0}{4\pi}\widehat{z}\times(ik_z\widehat{z}\times\vec{B}'\\ &= -\frac{B_0}{4\pi}ik_z(B'_z\widehat{z}-\vec{B}')\\ &= \frac{B_0}{4\pi}ik_z\vec{B}'_\perp\end{aligned}$$

Substitute in the **velocity equation**

$$\rho_0\partial_t\vec{u}+\nabla\cdot\left(\mathbf{p}'_{\rm gyro}+\mathbf{\Pi}\right)=\frac{1}{4\pi}(\nabla\times\vec{B}')\times(B_0\widehat{z})$$

and get

$$-i\omega\rho_0\vec{u}_\perp+(p_{0\|}-p_{0\perp})ik_z\frac{\vec{B}'_\perp}{B_0}+\frac{1}{\Omega}(2p_{0\|}-p_{0\perp})(ik_z)^2\widehat{z}\times\vec{u}_\perp=\frac{B_0}{4\pi}ik_z\vec{B}'_\perp$$

where the velocity is expressed from the induction equation

$$\vec{u}_\perp=-\frac{\omega}{k_z}\frac{\vec{B}'_\perp}{B_0}+\frac{v_A^2}{\Omega}(ik_z)\widehat{z}\times\frac{\vec{B}'_\perp}{B_0}$$

After substitution,

$$\left[\frac{\omega^2}{k_z^2}+\left(\frac{p_{0\parallel}-p_{0\perp}}{\rho_0}-v_A^2\right)\right]\frac{\vec{B}'_\perp}{B_0}-\frac{i\omega}{\Omega}\left(\frac{2p_{0\parallel}-p_{0\perp}}{\rho_0}+v_A^2\right)\hat{z}\times\frac{\vec{B}'_\perp}{B_0}=0$$

$$v_{th\parallel}^2=2\frac{p_{0\parallel}}{\rho_0}\qquad\qquad\beta_\parallel=\frac{v_{th\parallel}^2}{v_A^2}=\frac{8\pi p_{0\parallel}}{B_0^2}$$

$$\left[\frac{\omega^2}{v_{th\parallel}^2k_z^2}-\frac{1}{2}\left(\frac{T_{0\perp}}{T_{0\parallel}}-1+\frac{2}{\beta_\parallel}\right)\right]\frac{\vec{B}'_\perp}{B_0}-\frac{i\omega}{2\Omega}\left(2-\frac{T_{0\perp}}{T_{0\parallel}}+\frac{2}{\beta_\parallel}\right)\hat{z}\times\frac{\vec{B}'_\perp}{B_0}=0$$

Define

$$\overline{\omega}=\frac{\omega}{\Omega}\qquad\overline{k}_z=\frac{k_zv_{th\parallel}}{\Omega}$$

$$\left[\frac{\overline{\omega}^2}{\overline{k}_z{}^2}-\frac{1}{2}\left(\frac{T_{0\perp}}{T_{0\parallel}}-1+\frac{2}{\beta_\parallel}\right)\right]\frac{\vec{B}'_\perp}{B_0}-\frac{i\overline{\omega}}{2}\left(2-\frac{T_{0\perp}}{T_{0\parallel}}+\frac{2}{\beta_\parallel}\right)\hat{z}\times\frac{\vec{B}'_\perp}{B_0}=0$$

Solvability condition

$$\left[\frac{\overline{\omega}^2}{\overline{k}_z{}^2}-\frac{1}{2}\left(\frac{T_{0\perp}}{T_{0\parallel}}-1+\frac{2}{\beta_\parallel}\right)\right]^2-\frac{\overline{\omega}^2}{4}\left(2-\frac{T_{0\perp}}{T_{0\parallel}}+\frac{2}{\beta_\parallel}\right)^2=0$$

$$A=\frac{T_{0\perp}}{T_{0\parallel}}-1 \qquad\qquad \delta=A-\frac{2}{\beta_\parallel}$$

$$\overline{\omega}^2\pm\frac{\overline{k}_z{}^2}{2}(1-\delta)\overline{\omega}-\frac{\overline{k}_z{}^2}{2}\left(A+\frac{2}{\beta_\parallel}\right)=0$$

Instability if

$$A+\frac{2}{\beta_\parallel}<0$$

$$\overline{\omega}=\frac{\overline{k}_z{}^2}{4}(1-\delta)\pm i\frac{|\overline{k}_z|}{\sqrt{2}}\left[-\left(A+\frac{2}{\beta_\parallel}\right)-\frac{\overline{k}_z{}^2}{8}(1-\delta)^2\right]^{\frac{1}{2}}$$

real frequency

Unstable modes: $|\overline{k}_z|<\overline{k}_0$ with $\overline{k}_0=\frac{2\sqrt{2}}{|1-\delta|}\left|A+\frac{2}{\beta_\parallel}\right|^{\frac{1}{2}}$

$$\overline{k}_z=\frac{k_z v_{th\parallel}}{\Omega}$$

Schekochihin et al., Mon. Not. R. Astron. Soc. ***405****, 291, 2010*

Dispersive effects (Hall effect and pressure FLR corrections)

- induce a real part to the frequency (thus a velocity of propagation)
- arrest the instability at small scales

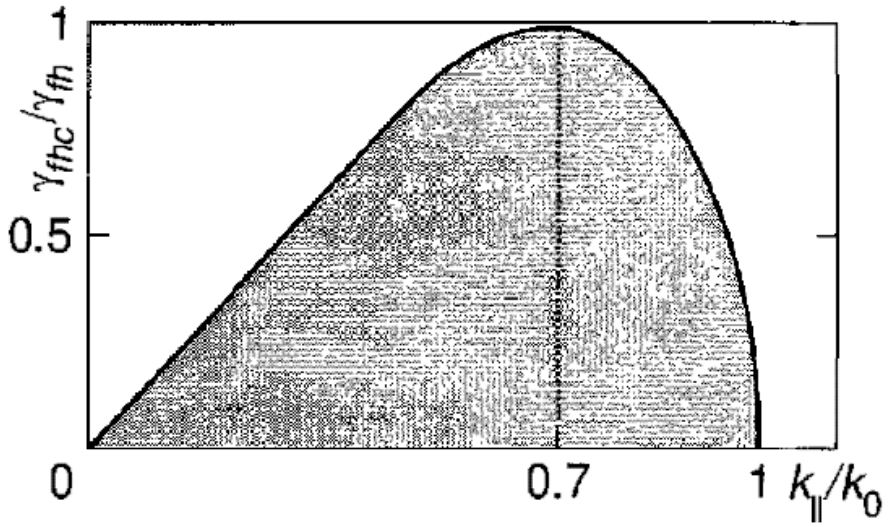

Fig. 3.8. Dependence of the firehose growth rate on wavenumber.

Influence of electron temperature anisotropy (arising in the generalized Ohm's low) can easily be taken into account

(Schekochihin et al., Mon. Not. R. Astron. Soc. ***405****, 291, 2010).*

Nonlinear saturation of the parallel (or whistler) fire-hose instability

Hybrid PIC simulations indicate a non-linear saturation in a **quasi-linear** manner (*Quest and Shapiro, JGR **101**, 24457, 1996; Gary et al. JGR **103**, 14567, 1998)*.

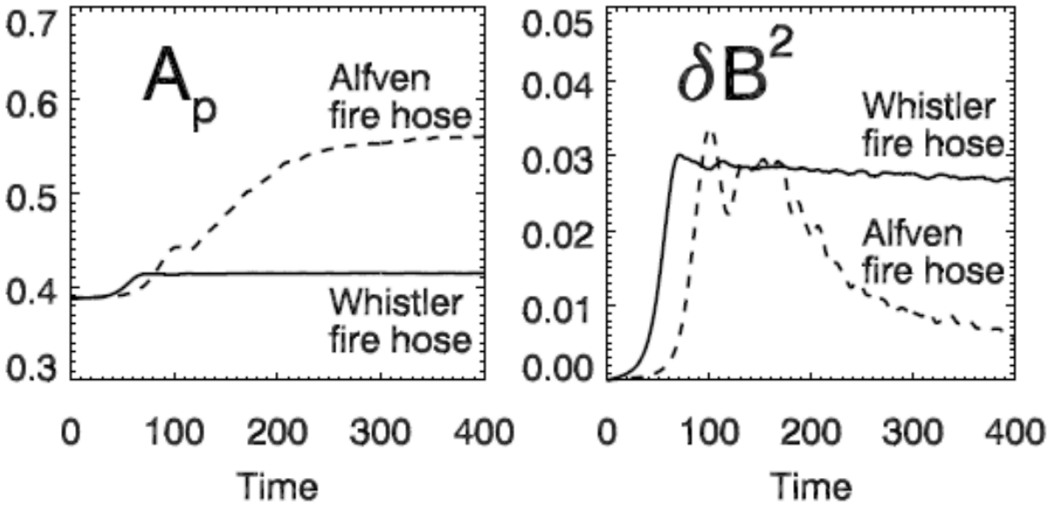

Figure 1. Simulation results for initial conditions $\beta_{p\|} = 2.8$ and $T_{p\perp}/T_{p\|} = 0.4$: Evolution of (left) temperature anisotropy $A_p = T_{p\perp}/T_{p\|}$ and (right) magnetic fluctuation δB^2 for the whistler fire hose (solid curve) at $\theta_{kB} = 0°$ and the Alfvén fire hose (dashed curve) at $\theta_{kB} = 53°$.

*Hellinger & Matsumoto, JGR **105**, 10519, 2000*

Figure 1 illustrates the fact that the whistler fire hose has a quasi-linear evolution (right panel): Magnetic fluctuation saturates at a certain level and stays at about this level after the saturation. The anisotropy slightly decreases to a level where the destabilized waves are marginally stable.

Nonlinear saturation of the parallel fire-hose instability (PIC simulations)

*Matteini et al. JGR **111**, A 10101, 2006.*

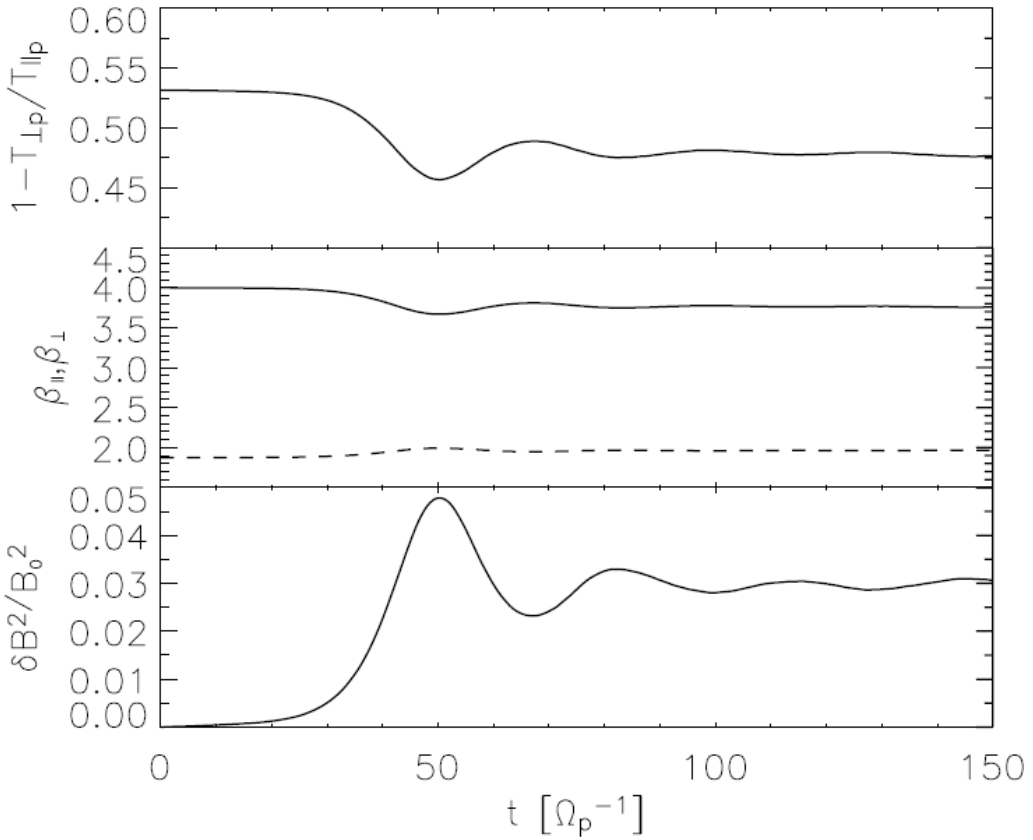

standard run (initial conditions $\beta_{\|p} = 4$, $1 - T_{\perp p}/T_{\|p} = 0.53$). We show the time evolution of: (top) the temperature anisotropy $1 - T_{\perp p}/T_{\|p}$; (center) $\beta_{\|p}$ (solid line) and $\beta_{\perp p}$ (dashed line); (bottom) variation of the magnetic fluctuations $\delta B^2/B_0^2$. $\beta_e = 1$.

After the parallel fire hose has saturated, the system is in a condition of marginal stability. Note that in the final state $\beta_{\|p} - \beta_{\perp p} < 2$; as $\beta_{\|p} - \beta_{\perp p} = 2$ is the saturation value predicted by the fluid-CGL nonresonant description, this confirms a resonant behavior during the stabilization.

The fluid theory is valid only very close to the instability threshold.
It requires that for the most unstable mode,

$$|\zeta_p^{\pm}| = \left| \frac{\omega \pm \Omega_p}{\sqrt{2} k_{\|} v_{th\|p}} \right| \gg 1$$

$$\Omega_p = \frac{eB_0}{m_p c}$$

Ion gyrofrequency

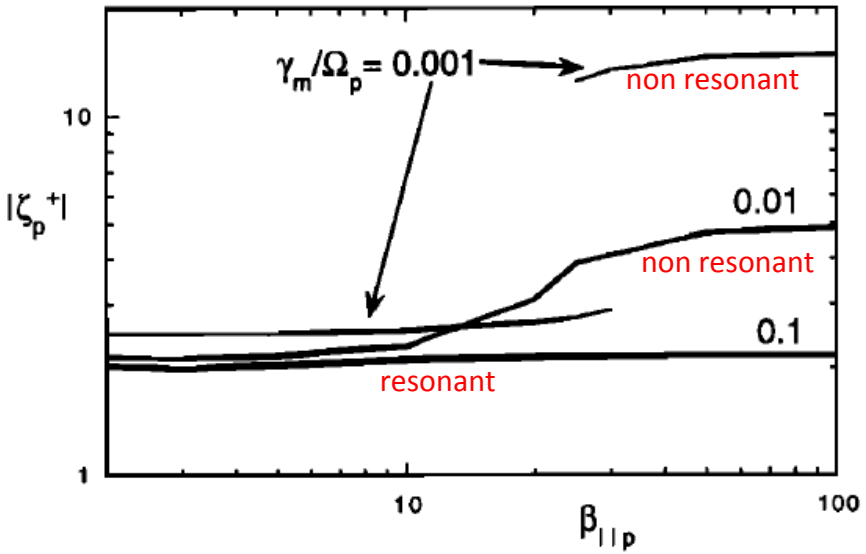

Figure 2. Linear theory results: the proton cyclotron resonance factor at the wavenumber of maximum growth of the proton firehose instability as a function of the parallel proton β for three values of the maximum growth rate.

*Gary et al. JGR, **103**, 14574, 1998*

From kinetic theory

Resonances affects the instability threshold

The right-handed polarized whistler mode is destabilized.

Under resonant conditions, the linear threshold condition for a fixed value of the dimensionless maximum growth rate γ_m / Ω_p of the proton firehose instability in an electron-proton plasma can be written for $\gamma_m / \Omega_p < 0.10$ as

$$1 - \frac{T_{\perp p}}{T_{\|p}} = \frac{S_p}{\beta_{\|p}{}^{\alpha_p}}$$

over $1 \le \beta_{\|p} \le 10$.

S_p is a dimensionless number of order unity determined by the choice of the maximum growth rate, but $\alpha_p \simeq 0.7$, relatively independent of γ_m / Ω_p.

Resonances enlarge the instability region

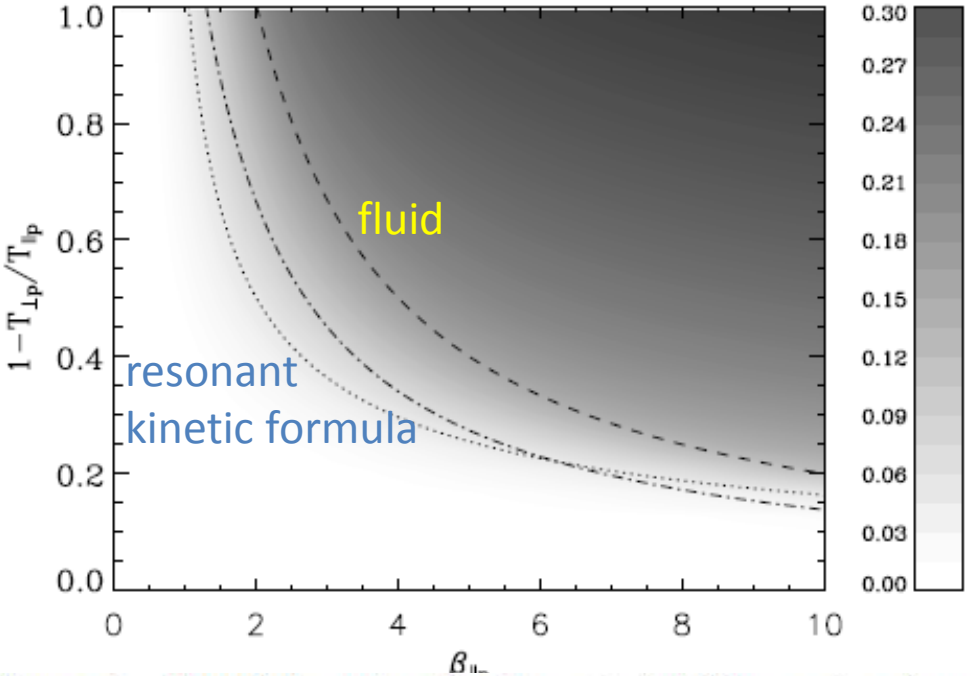

Figure 1. Parallel proton fire hose instability region from linear analysis in the parameter space ($\beta_{\|p}$, $1 - T_{\perp p}/T_{\|p}$). The grey encodes the maximum instability growth rate: the white region is stable whereas the grey region is unstable and darker intensity corresponds to stronger growth rates, according to the scale shown on the right. The dotted line corresponds to the fitting of the unstable region using relation (5). For comparison the dash-dotted line corresponds to the analogous fitting for the oblique fire hose. The CGL non resonant threshold condition (dashed line) is also shown.

*Matteini et al. JGR **111**, A 10101, 2006.*

Resonances enlarge the instability region

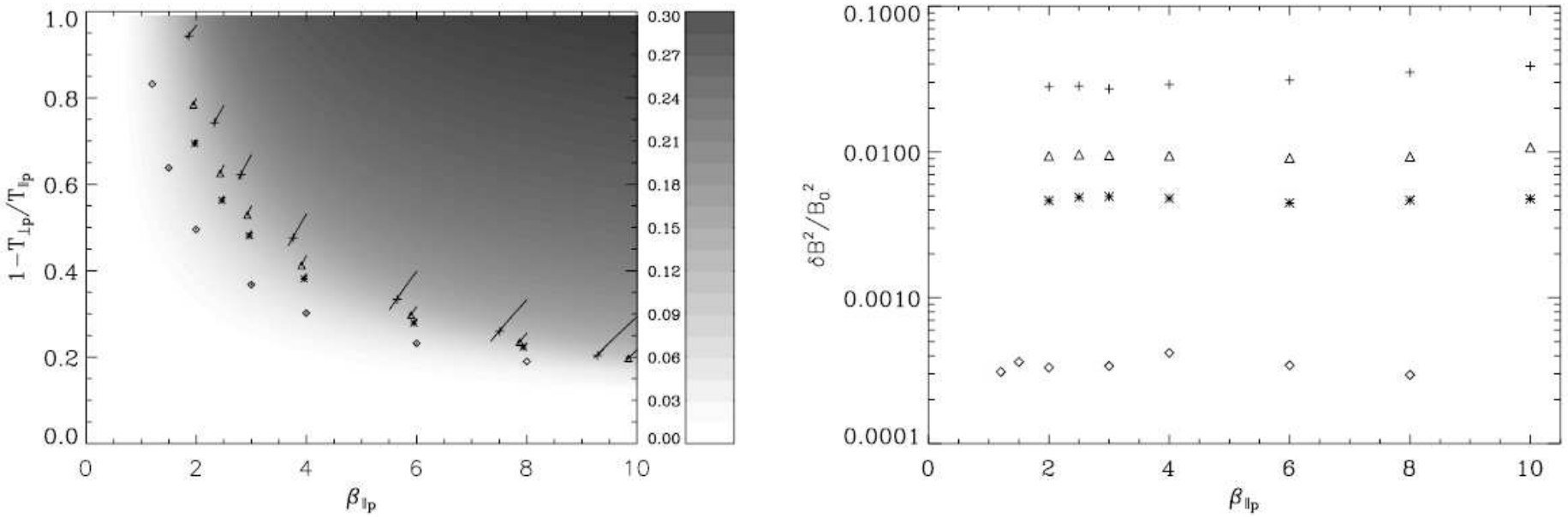

Figure 3. Results from hybrid simulations; the final post saturation states are denoted by crosses (γ_m = 0.1), triangles (γ_m = 0.05), stars (γ_m = 0.03) and diamonds (γ_m = 0.005). Left: solid lines are the trajectories in the plane ($\beta_{\parallel p}$, $1 - T_{\perp p}/T_{\parallel p}$) for each simulation. As in Figure 1, the linear analysis prediction is also shown. Right: Saturation levels of the magnetic fluctuation energy as a function of the proton parallel beta.

*Matteini et al. JGR **111**, A 10101, 2006.*

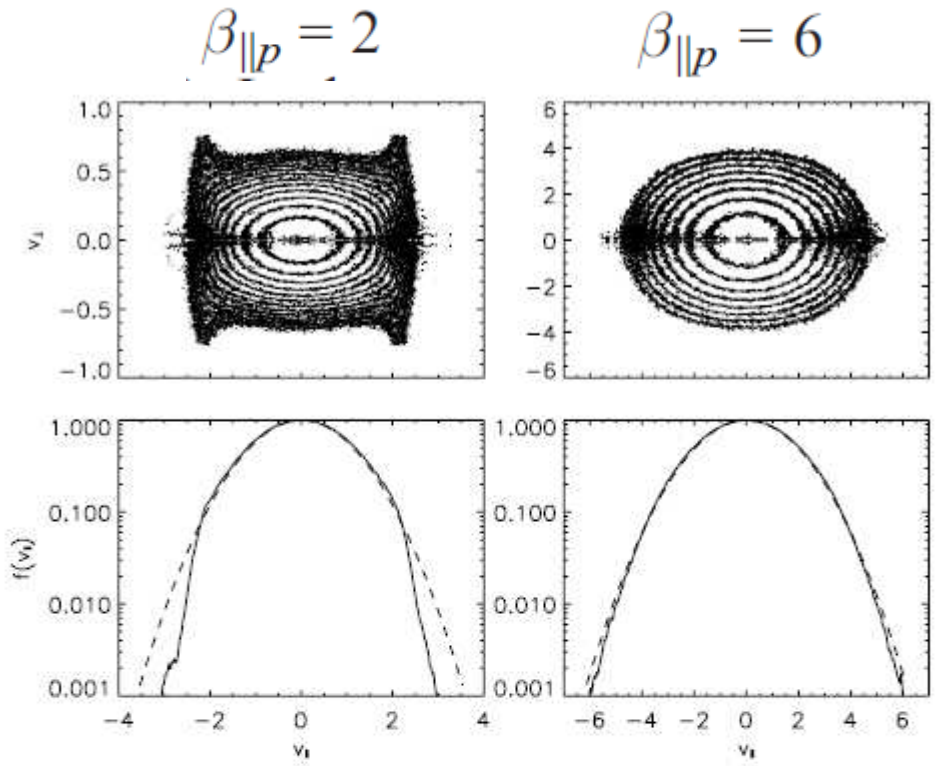

Figure 4. Proton distribution functions in the case $\beta_{\|p} = 2$ (left) and $\beta_{\|p} = 6$ (right) (f given in arbitrary units). In the top panels we show the final distribution function $f(v_{\|}, v_{\perp})$ in the plane of the parallel and perpendicular velocities. In the bottom panels we show in solid line the final parallel velocity distribution $f(v_{\|})$ after the stabilization; the Maxwellian distribution function associated to the temperature of the system in the final stable state has been plotted as reference (dashed line).

Proton velocity distribution function

The departure from the initial biMaxwellian is more important in the case of lower β.

The deformation of the velocity distribution function is a direct consequence of the resonant interaction of the protons with the waves.

*Matteini et al. ,JGR **111**, A 10101, 2006.*

Quasi-linear saturation of the fire-hose instability:

- Theory in the non-resonant regime: *Shapiro & Shevchenko, JETP **18**, 1109, 1964.*

  Predict asymptotic **relaxation to the marginal equilibrium condition** given by the fluid theory.

- Effect of weak collisions and also of turbulence: *Rosin et al., MNRAS **413**, 7, 2011.*

- Effect of the resonances: *Seough & Yoon, JGR **117**, A08101, 2012.*

A flavor of quasi-linear theory (see e.g. Diamond, Itoh & Itoh, *Modern Plasma Physics: Vol. 1, Physical Kinetics of Turbulent Plasmas*, Cambridge Univ. Press 2010).

$$\partial_t f + v\partial_x f + \frac{q}{m} E \partial_v f = 0$$

Separate **space-averaged** contributions from **fluctuations** (taken in the linear approximation)

$$f = \langle f \rangle + \delta f$$

$$\partial_t \langle f \rangle + \frac{q}{m} \partial_v \langle E \delta f \rangle = 0$$

$$\partial_t \delta f + v\partial_x \delta f + \frac{q}{m} E \partial_v \langle f \rangle = 0$$

$$E = \frac{1}{2} \sum_k (E_k e^{ikx} + c.c.)$$

$$\partial_t \langle f \rangle + \frac{q}{2m} \partial_v \sum_k \langle E_k^* \delta f_k + c.c. \rangle = 0$$

Assuming that the **fluctuations evolve much faster** than the electric field and the space-averaged distribution function,

$$-i(\omega - ikv)\delta f_k + \frac{q}{m} E_k \partial_v \langle f \rangle = 0$$

Here $\omega = \omega_k + i\gamma_k$ is viewed as the (complex) frequency of the considered kind of waves, given by the dispersion relation based on the instantaneous particle distribution function $\langle f \rangle$.

$$\delta f_k = -i\frac{q}{m}\frac{E_k \partial_v \langle f \rangle}{\omega - kv}$$

$$\boxed{\partial_t \langle f \rangle = \partial_v [D(v)\partial_v \langle f \rangle]}$$

$$D(v) = \frac{q^2}{m^2}\mathrm{Re}\sum_k \frac{i|E_k|^2}{\omega_k - kv + i|\gamma_k|}$$

$$\boxed{D(v) = \sum_k \frac{q^2}{m^2}|E_k|^2 \frac{|\gamma_k|}{(\omega_k - kv)^2 + \gamma_k^2}}$$

$$\boxed{\partial_t |E_k|^2 = 2\gamma_k |E_k|^2}$$ (growth rate calculated from <f(x,t)>)

The absolute value is aimed to cope with the case of damped modes.
This formula is valid in the limit $\Upsilon_k \to 0$, but additional terms arise otherwise *(Hellinger & Travnicek, PoP **19**, 062307, 2012*).

The oblique or Alfvén fire-hose instability

Hellinger & Matsumoto,
*JGR **105**, 10519, 2000*
*JGR **106**, 13215, 2001*

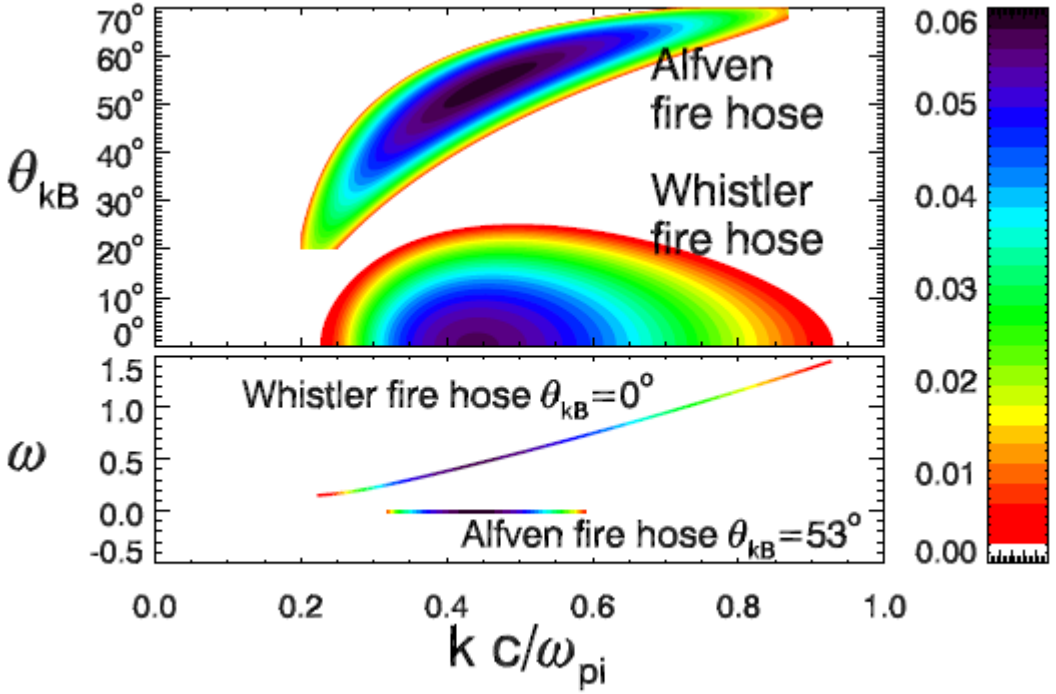

Plate 4. Linear theory, $\beta_{p\|} = 2.8$, $T_{p\perp}/T_{p\|} = 0.4$: (top) Growth rate $\gamma = \gamma(k, \theta_{kB})$ of the Alfvén and whistler fire hoses shown as a 2-D color scale plot. (the color scale used is displayed at right). (bottom) Frequency $\omega = \omega(k)$ of unstable waves for the whistler fire hose at $\theta_{kB} = 0°$ and the Alfvén fire hose at $\theta_{kB} = 53°$. The curves $\omega = \omega(k)$ are colored using the growth-rate color scale displayed at right.

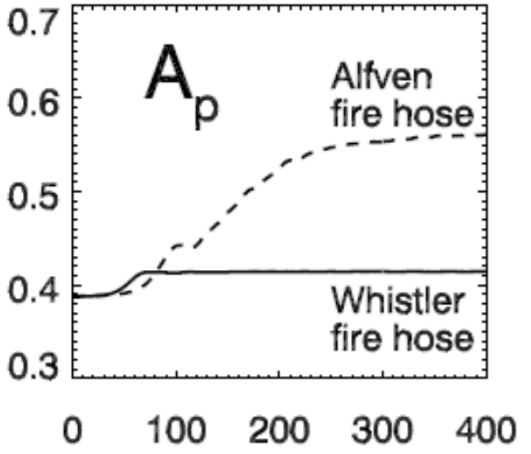

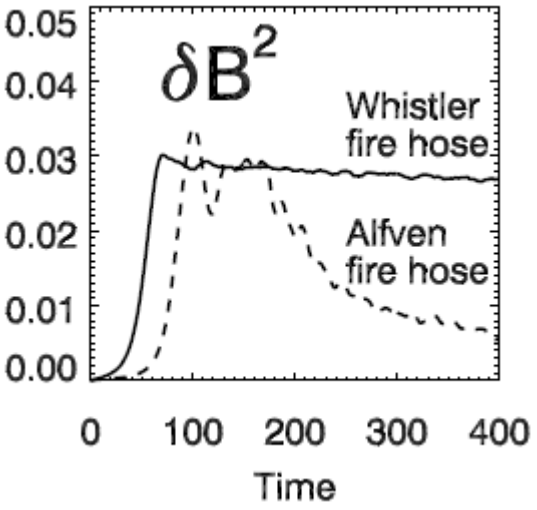

$A_p = T_{p\perp}/T_{p\|}$

See also *Wang & Hau, JGR **108**, 1463, 2003; Hau and Wang, NPG **14**, 557, 2007*

The oblique or Alfvén fire-hose instability

(Empirical) threshold: $\beta_{p\|}(1 - T_{p\perp}/T_{p\|}) \sim 1.4$ for $2 < \beta_{p\|} < 4$, $\beta_{\|} - \beta_{\perp} \approx 1.4$

- Zero-frequency mode (purely growing)
- Resonant instability *(Hellinger & Travnicek, JGR **113**, 10109, 2008)*
- Maximum growth rate at oblique propagation
- Linear polarization: $\delta B = \delta B n$ (where n is a unit vector parallel to $k \times B_0$)
- Compressible mode: $(\delta n/n)/(|\delta B|/B_0) \sim 0.1$
- Anti-correlated density and magnetic field fluctuations

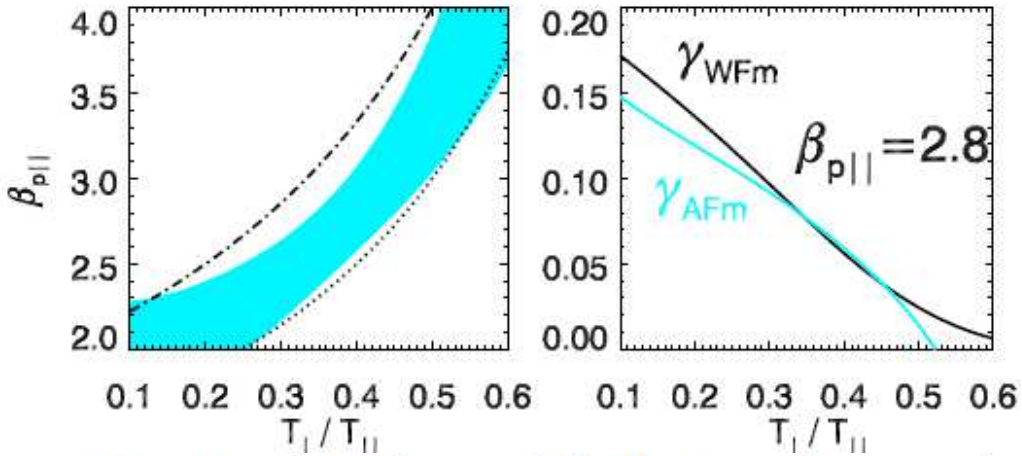

Plate 3. Linear theory: (left) Blue area shows a region in $(T_{p\perp}/T_{p\|}, \beta_{p\|})$ space where the maximum growth rate of the Alfvén fire hose γ_{AFm} is greater than the maximum growth rate of the whistler fire hose γ_{WFm}. Overlain curves denote the relations $\beta_{p\|}(1 - T_{p\perp}/T_{p\|})$ equal to 2 (dash-dotted curve) and 1.5 (dotted curve). (right) Maximum growth rates γ_{WFm} (black curve) and γ_{WFm} (blue curve) as a function of $T_{p\perp}/T_{p\|}$ for $\beta_{p\|} = 2.8$

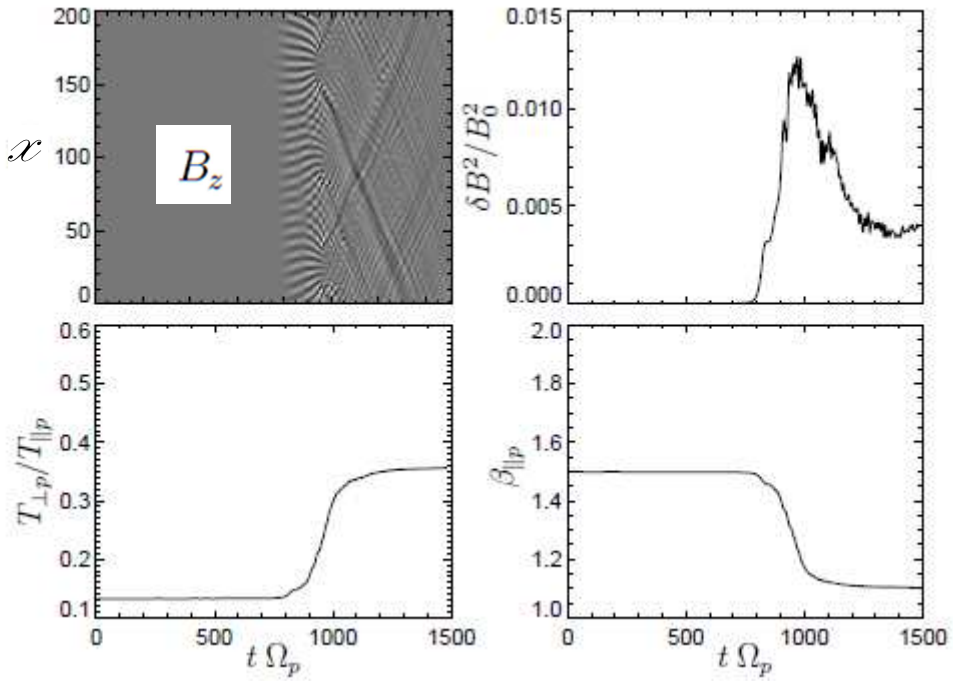

*Hellinger &Travnicek, JGR **113**, A10109, 2008*

No quasi-linear relaxation to marginal equilibrium, but Alfvén wave damping and heating of the protons.

Figure 1. Evolution in run 1 (see Table 1): (left top) Gray scale plot of B_z as a function of time and x (only a part of the simulation box is shown). (right top) The fluctuating magnetic energy $\delta B^2/B_0^2$ as function of time. (left bottom) The proton temperature anisotropy $T_{\perp p}/T_{\parallel p}$ as a function of time. (bottom right) The parallel proton beta $\beta_{\parallel p}$ a function of time.

Table 1. Initial conditions for the set of 1-D standard hybrid simulations

Run #	γ_m/Ω_p	$\beta_{\parallel p}$	$T_{\perp p}/T_{\parallel p}$	$k_m c/\omega_p$	θ_m
1		1.5	0.134	0.714	56.1°

Mirror instability

Return to the case of arbitrary perturbations (concentrate on largest scales)

$$\begin{cases} -\rho_0\omega^2\xi_x + ik_x p'_\perp - (p_{0\parallel} - p_{0\perp})k_z^2\xi_x + \dfrac{B_0^2}{4\pi}(k_x^2 + k_z^2)\xi_x = 0 \\ -\rho_0\omega^2\xi_y - (p_{0\parallel} - p_{0\perp})k_z^2\xi_y + \dfrac{B_0^2}{4\pi}k_z^2\xi_y = 0 \\ -\rho_0\omega^2\xi_z + ik_z p'_\parallel - (p_{0\parallel} - p_{0\perp})k_x k_z\xi_x = 0 \end{cases}$$

Simplest closure: double adiabatic (or CGL) approximation: prescribes zero heat fluxes.

This leads to prescribe the equations of state:

$$\frac{p_\perp}{\rho B} = \text{cst} \qquad \frac{p_\parallel B^2}{\rho^3} = \text{cst}$$

or

$$\frac{p'_\perp}{p_{0\perp}} = \frac{\rho'}{\rho_0} + \frac{B'}{B_0} \qquad \frac{p'_\parallel}{p_{0\parallel}} = 3\frac{\rho'}{\rho_0} - 2\frac{B'}{B_0}$$

$$\frac{B'}{B_0} = -ik_x\xi_x$$

$$\partial_t\rho' + i\vec{k}\cdot(\rho_0\partial_t\vec{\xi}) = 0 \qquad \text{gives} \qquad \frac{\rho'}{\rho_0} = -i(k_x\xi_x + k_z\xi_z)$$

$$\frac{p'_\perp}{p_{0\perp}} = -2ik_x\xi_x - ik_z\xi_z$$

$$\frac{p'_\parallel}{p_{0\parallel}} = -ik_x\xi_x - 3ik_z\xi_z$$

$$\left[-\rho_0\omega^2 + 2k_x^2\left(p_{0\perp} + \frac{B_0^2}{8\pi}\right) + k_z^2\left(p_{0\perp} - p_{0\parallel} + \frac{B_0^2}{4\pi}\right)\right]\xi_x + k_xk_zp_{0\perp}\xi_z = 0$$

$$k_xk_zp_{0\perp}\xi_x + \left[-\rho_0\omega^2 + 3p_{0\parallel}k_z^2\right]\xi_z = 0$$

Solvability:

$$\rho_0^2\omega^4 - \rho_0\omega^2\left[p_{0\perp}(2k_x^2 + k_z^2) + \frac{B_0^2}{4\pi}(k_x^2 + k_z^2) + 2p_{0\parallel}k_z^2\right]$$
$$+3p_{0\parallel}k_z^2\left\{2k_x^2\left[\frac{B_0^2}{8\pi} + p_{0\perp}\left(1 - \frac{p_{0\perp}}{6p_{0\parallel}}\right)\right] + k_z^2\left(\frac{B_0^2}{4\pi} + p_{0\perp} - p_{0\parallel}\right)\right\}$$
$$= 0$$

For quasi –transverse directions

$\omega^2 < 0$ if $\quad p_{0\perp}\left(1 - \frac{p_{0\perp}}{6p_{0\parallel}}\right) + \frac{B_0^2}{8\pi} < 0$

Instability condition: $\quad \frac{p_{0\perp}}{6p_{0\parallel}} - 1 - \frac{1}{\beta_\perp} > 0$

which differs from the kinetic prediction by the factor 6.

The correct stability threshold

$$\frac{p_{0\perp}}{p_{0\parallel}} - 1 - \frac{1}{\beta_\perp} > 0$$

can be obtained by performing a quasi-normal (QN) closure of the fluid hierarchy
(i.e. retaining heat fluxes but neglecting fourth rank cumulants)
*(Passot, Ruban & Sulem, PoP **13**, 102310 2006;*
*Dzhalilov, V.D. Kuznetsov & J. Staude, Contrib. Plasma Phys**. 51**, 621, 2010*).

This QN closure may be suitable for analyzing stationary solutions but
cannot correctly reproduce the time dynamics.

In fact**, advection terms are negligible (pressure equilibrium),** with **time dependency originating from Landau damping.**

The physics of the mirror instability

(from Treumann & Baumjohann Advanced Space Plasma Physics, 1997)

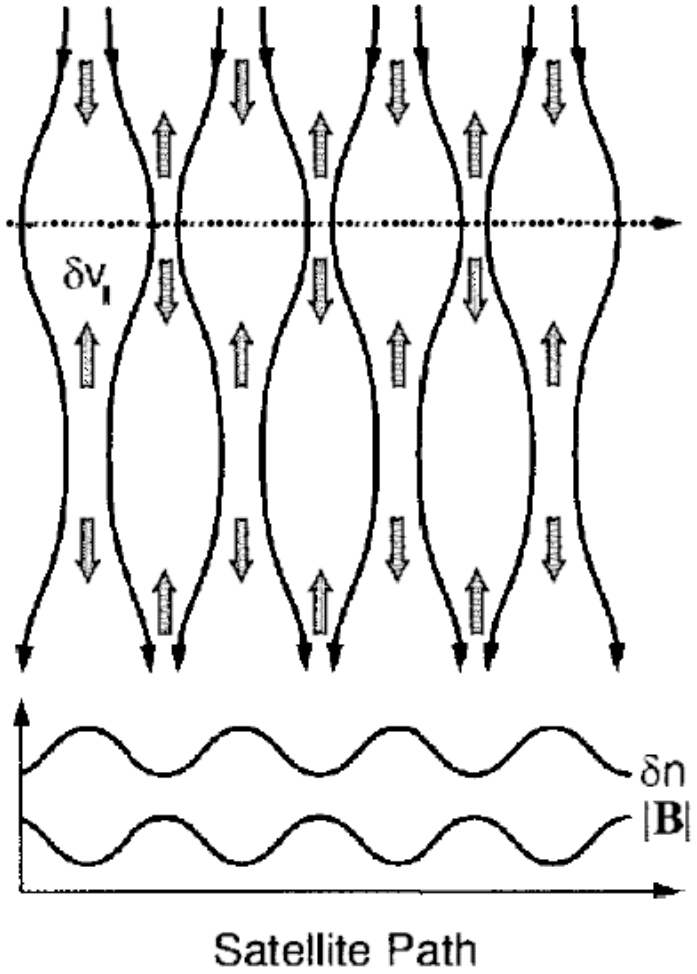

Fig. 3.9. Satellite measurements across a mirror-unstable region.

The particles become trapped in the magnetic configurations whenever, under the action of large perpendicular pressure, the magnetic field locally inflates over one wavelength.

In this bottle, the particle perform a mirror motion between the knots of the wave.

Particles stream into the mirror during the instability.

The whole region consists of magnetic mirrors which, when crossed by a spacescraft, are recorded as pulsation of oscillations of the magnetic field and out-of-phase oscillations of the density.

See also *Southwood & Kivelson, JGR **98**, 9181, 1993*
*Kivelson & Southwood, JGR **101**, 17365, 1996*

A kinetic approach is required for a quantitative analysis of the mirror instability, but a mixed description is in fact convenient to evaluate the various contributions.

Assume cold electrons

$$\rho\frac{du_i}{dt} = -\partial_j\left[\left(p_\perp + \frac{|B|^2}{8\pi}\right)\delta_{ij} - \left(p_\perp - p_\parallel + \frac{|B|^2}{4\pi}\right)\widehat{b}_i\widehat{b}_j + \Pi_{ij}\right]$$

$$\rho\frac{d\vec{u}}{dt} = -\nabla\left(p_\perp + \frac{|B|^2}{8\pi}\right) + \left(1 + \frac{4\pi}{|B|^2}(p_\perp - p_\parallel)\right)\frac{\vec{B}\cdot\nabla\vec{B}}{4\pi}$$
$$-\widehat{b}\frac{|B|^2}{4\pi}(\widehat{b}\cdot\nabla)\left(1 + \frac{4\pi}{|B|^2}(p_\perp - p_\parallel)\right) - \nabla\cdot\mathbf{\Pi}.$$

Scaling: $\nabla_\perp \sim \varepsilon^{\frac{1}{2}}$, $\partial_z \sim \varepsilon$, $\partial_t \sim \varepsilon^2$, where ε measures the distance to threshold.

The advection term is subdominant: pressure balance equilibrium

Project on the plane perpendicular to the local magnetic field and linearize.

$$-\nabla_\perp\left(p'_\perp+\frac{B_0B_z}{4\pi}\right)+\left(1+\frac{4\pi}{B_0^2}(p_{0\perp}-p_{0\parallel})\right)\frac{B_0}{4\pi}\partial_z\vec{B}_\perp-(\nabla\cdot\mathbf{\Pi})_\perp=0$$

Time dependence will arise, through the perpendicular pressure, from **Landau damping**.

Kinetic theory $\boxed{j_z=0}$ or $\nabla_\perp\times\vec{B}_\perp=0$ or $\nabla_\perp\times(\nabla_\perp\times\vec{B}_\perp)=0$

$$\nabla_\perp(\nabla_\perp\cdot\vec{B}_\perp)-\Delta_\perp\vec{B}_\perp=0$$

Using $\nabla\cdot\vec{B}=0$

$$\vec{B}_\perp=(-\Delta_\perp)^{-1}\nabla_\perp\partial_z B_z$$

$$\boxed{\nabla_\perp\left[p'_\perp+\frac{B_0B_z}{4\pi}+\frac{2}{\beta_\perp}\left(1+\frac{\beta_\perp-\beta_\parallel}{2}\right)p_{0\perp}\frac{\partial_{ZZ}}{\Delta_\perp}\frac{B_z}{B_0}\right]+\left(\nabla\cdot\mathbf{\Pi}\right)_\perp=0}$$

Linear kinetic theory near a bi-Maxwellian equilibrium : *Califano et al., JGR **113**, A08219, 2008*

$$p'_\perp = \beta_\perp \left(1 - \frac{\beta_\perp}{\beta_\parallel}\right) \frac{B_0 B'_z}{4\pi} + \frac{\sqrt{\pi}}{v_{th\,\parallel}} \partial_t \left(-\mathcal{H}\,\partial_z\right)^{-1} \frac{\beta_\perp^2}{\beta_\parallel} \frac{B_0 B_z}{4\pi}$$
$$- p_{0\perp} \frac{9}{4\beta_\perp} r_L^2 \Delta_\perp \frac{B_z}{B_0}$$

time derivative

$$\left(\nabla \cdot \mathbf{\Pi}\right)_\perp = -\frac{3}{4}\left(1 - \frac{\beta_\perp}{\beta_\parallel}\right) p_{0\perp} r_L^2 \Delta_\perp \nabla_\perp \frac{B_z}{B_0}$$

Hilbert operator

$$\text{Fourier}\{-\mathcal{H}\} = \frac{ik_z}{|k_z|}$$

signature of Landau resonance

$$r_L = \frac{v_{th\perp}}{\Omega} = \frac{1}{\Omega}\sqrt{\frac{2T_{0\perp}}{m}}$$

ion Larmor radius

To be substituted in the pressure balance equation.

After substitution in the pressure balance equation,

$$\partial_t B_z(\vec{k},t) = \gamma_{\vec{k}} B_z(\vec{k},t)$$

$$\gamma_{\vec{k}} = |k_z| v_{th\parallel} \frac{\beta_\parallel}{\sqrt{\pi}\beta_\perp}\left[\frac{\beta_\perp}{\beta_\parallel} - 1 - \frac{1}{\beta_\perp} - \frac{1}{\beta_\perp}\left(1 + \frac{\beta_\perp - \beta_\parallel}{2}\right)\frac{k_z^2}{k_\perp^2} - \frac{3}{4\beta_\perp}k_\perp^2 r_L^2\right]$$

Instability condition:

$$\frac{\beta_\perp}{\beta_\parallel} - \frac{1}{\beta_\perp} > 1$$

The arrest of the instability at small scales originates from FLR corrections

- Non-gyrotropic pressure:

$$\frac{3}{4}\left(1 - \frac{\beta_\perp}{\beta_\parallel}\right) p_{0\perp} k_\perp^2 r_L^2 \approx -\frac{3}{4\beta_\perp} p_{0\perp} k_\perp^2 r_L^2$$

- FLR contribution to the perpendicular (gyrotropic) pressure:

$$\frac{9}{4\beta_\perp} p_{0\perp} r_L^2 k_\perp^2$$

In fact a destabilizing effect

This approach can easily be extended to retain nonlinear contributions
(which at this order of expansion are purely hydrodynamic, with no FLR contributions).

General case of hot electrons:

Linear instability more easily studied in a **fully kinetic framework**, using

Electric quasi-neutrality: $n_i - n_e = 0$

Linearized Ampère equation: $\vec{j} = en_0(\vec{u}_i - \vec{u}_e)$

- $en_0 \nabla_\perp \times (\vec{u}_{i\perp} - \vec{u}_{e_\perp}) = \nabla_\perp \times \vec{j}_\perp = \frac{c}{4\pi} \Delta(b_z \hat{z})$
- $\vec{u}_{\perp r} = -\nabla_\perp \chi_{cr} + \nabla_\perp \times (\chi_{sr} \hat{z}) \qquad r = i \text{ or } e$

$$\Longrightarrow \quad \Delta b_z = \frac{4\pi e n_0}{c B_0} \Delta_\perp (\chi_{si} - \chi_{se})$$

*Kuznetsov, Passot, & Sulem, PoP **19**, 092116, 2012*

Need kinetic expressions for n_r, u_{zr} and χ_{zr}.

The computations are strongly simplified in prescribing a **priori a low-frequency, quasi-transverse asymptotics** (instead of deriving general formulas and taking limits afterwards, e.g. *Pokhotelov et al., Adv. Space Res.* ***37****, 1550, 2006*).

The various quantities are expressed in term of the parallel magnetic field perturbation b_z and of the potentials Φ and Ψ defined by

$$k^2(\Phi - \Psi) = \frac{4\pi}{c^2}\frac{\omega}{k_z} j_z$$

$$E_z = -ik_z \Psi$$

$$\mathfrak{M}\vec{X} = 0 \begin{cases} X_1 = \dfrac{b_z}{B_0} \\ X_2 = \dfrac{e}{T_{\perp i}}(1 + \dfrac{k_z^2}{k^2})(\Phi - \Psi) \\ X_3 = \dfrac{e\Psi}{T_{\parallel i}} \end{cases}$$

After multiplying the 2nd line by k_z/ω

In the special case of isotropic equilibrium temperatures, the matrix reduces to that derived from the gyrokinetic theory by *Howes et al. ApJ* ***651****, 590,* 2006 for computing KAW's dispersion relation.

$$\mathfrak{M}_{11} = -(\Gamma_0(b_i) - \Gamma_1(b_i))\Big(\frac{T_{\perp i}}{T_{\parallel i}}R(\zeta_i) - 1\Big) + (\Gamma_0(b_e) - \Gamma_1(b_e))\Big(\frac{T_{\perp e}}{T_{\parallel e}}R(\zeta_e) - 1\Big)$$

$$\mathfrak{M}_{12} = \Gamma_0(b_i) - 1 + \frac{T_{\perp i}}{T_{\perp e}}(\Gamma_0(b_e) - 1)$$

$$\mathfrak{M}_{13} = -\Big[\Gamma_0(b_i)R(\zeta_i) + \frac{T_{\parallel i}}{T_{\perp i}}(1 - \Gamma_0(b_i))\Big] - \Big[\Gamma_0(b_e)R(\zeta_e) + \frac{T_{\parallel e}}{T_{\perp e}}(1 - \Gamma_0(b_e))\Big]\frac{T_{\parallel i}}{T_{\parallel e}}$$

$$\mathfrak{M}_{21} = (\Gamma_1(b_i) - \Gamma_0(b_i))\frac{T_{\perp i}}{T_{\parallel i}}R(\zeta_i) - (\Gamma_1(b_e) - \Gamma_0(b_e))\frac{T_{\perp e}}{T_{\parallel e}}R(\zeta_e)$$

$$\mathfrak{M}_{22} = -\frac{1}{2\zeta_i^2}\Big[\Big(\frac{T_{\perp i}}{T_{\parallel i}} - 1\Big)(1 - \Gamma_0(b_i)) + \frac{T_{\perp i}}{T_{\parallel i}}\frac{v_A^2}{\Omega_i^2}k_\perp^2 + \frac{m_i}{m_e}\frac{T_{\parallel e}}{T_{\perp e}}\frac{T_{\perp i}}{T_{\parallel i}}\Big(\frac{T_{\perp e}}{T_{\parallel e}} - 1\Big)(1 - \Gamma_0(b_e))\Big]$$

$$\mathfrak{M}_{23} = -\Big[\Gamma_0(b_i)R(\zeta_i) + \frac{T_{\parallel i}}{T_{\parallel e}}\Gamma_0(b_e)R(\zeta_e)\Big]$$

$$\mathfrak{M}_{31} = \beta_{\perp i}(\Gamma_0(b_i) - \Gamma_1(b_i))\Big(\frac{T_{\perp i}}{T_{\parallel i}}R(\zeta_i) - 1\Big) + \beta_{\perp e}\Big(\Gamma_0(b_e) - \Gamma_1(b_e))(\frac{T_{\perp e}}{T_{\parallel e}}R(\zeta_e)) - 1\Big) - 1 - \Big[1 + \frac{1}{2}(\beta_{\perp i} - \beta_{\parallel i} + \beta_{\perp e} - \beta_{\parallel e})\Big]\frac{k_z^2}{k_\perp^2}$$

$$\mathfrak{M}_{32} = -\frac{\beta_{\perp i}}{2}\Big(\Gamma_0(b_i) - \Gamma_1(b_i) - \Gamma_0(b_e) + \Gamma_1(b_e)\Big)$$

$$\mathfrak{M}_{33} = \frac{\beta_{\parallel i}}{2}\Big[(\Gamma_0(b_i) - \Gamma_1(b_i))\Big(\frac{T_{\perp i}}{T_{\parallel i}}R(\zeta_i) - 1\Big) - (\Gamma_0(b_e) - \Gamma_1(b_e))\Big(\frac{T_{\perp e}}{T_{\parallel e}}R(\zeta_e)) - 1\Big)\Big],$$

$$\zeta_r = \frac{\omega}{|k_z|v_{\mathrm{th}\parallel r}}$$

$$R(\zeta_r) = 1 + i\sqrt{\pi}\xi_r - 2\zeta_r^2 + O(\zeta_r^3)$$

Low-frequency dynamics

Retaining the first (second) order leads to a dispersion relation in the form of a **first (second) degree polynomial**.

$$b_r = k_\perp^2\frac{T_{\perp r}}{m_r\Omega_r^2}$$

$$\Gamma_\nu(b_r) = e^{-b_r}I_\nu(b_r)$$

Modified Bessel function of order *v*

When the instability is confined at large scale:

- Neglect electron Landau damping $R(\zeta_e) = 1$
- Neglect electron FLR corrections $\Gamma_0(b_e) = 1$
- Expand the ion quantities:

$$\Gamma_0(b) = 1 - b + \frac{3}{4}b^2 + O(b^3) \qquad \Gamma_1(b) = \frac{b}{2} - \frac{b^2}{2} + O(b^3)$$

$$R(\zeta_i) = 1 + i\sqrt{\pi}\zeta_i + O(\zeta_i^2)$$

Solvability condition: $$\Lambda_1 + \Lambda_2 \frac{k_z^2}{k_\perp^2} + \Lambda_3 \frac{i\sqrt{\pi}}{v_{\text{th}}} \frac{\omega}{|k_z|} + \Lambda_4 b = 0$$

$$\Lambda_1 = \frac{1}{\beta_{\perp i}} \left[\beta_{\perp i} \left(\frac{T_{\perp i}}{T_{\parallel i}} - 1 \right) + \beta_{\perp e} \left(\frac{T_{\perp e}}{T_{\parallel e}} - 1 \right) - 1 - \frac{1}{2} \frac{\left(\frac{T_{\perp i}}{T_{\parallel i}} - \frac{T_{\perp e}}{T_{\parallel e}} \right)^2}{\frac{1}{\beta_{\parallel i}} + \frac{1}{\beta_{\parallel e}}} \right]$$

Threshold:

$$\beta_{\perp i} \left(\frac{T_{\perp i}}{T_{\parallel i}} - 1 \right) + \beta_{\perp e} \left(\frac{T_{\perp e}}{T_{\parallel e}} - 1 \right) - 1 - \frac{1}{2} \frac{\left(\frac{T_{\perp i}}{T_{\parallel i}} - \frac{T_{\perp e}}{T_{\parallel e}} \right)^2}{\frac{1}{\beta_{\parallel i}} + \frac{1}{\beta_{\parallel e}}} = 0$$

Growth rate:

$$\gamma = \frac{2}{\sqrt{\pi}}\frac{T_{\|i}}{T_{\perp i}}\frac{|k_z|v_{th\|i}}{D} \times \left\{\frac{T_{\perp i}}{T_{\|i}}\frac{C}{2} - (1+\theta_\perp)\left[1+\frac{1}{\beta_\perp}+\frac{1}{\beta_\perp}\left(1+\frac{\beta_\perp-\beta_\|}{2}\right)\frac{k_z^2}{k_\perp^2}\right] - \frac{3}{4}\left(\frac{T_{\perp i}}{T_{\|i}}-1\right)(1+B)k_\perp^2 r_L^2\right\}.$$

$$C = \frac{(\theta_\perp+\theta_\|)^2 + 2\theta_\|(\theta_\perp^2+1)}{\theta_\|(\theta_\|+1)}$$

$$1+B = \frac{3(1+\theta_\|+\theta_\perp)+(\theta_\perp^2+\theta_\perp\theta_\|+\theta_\|^2)}{3(1+\theta_\|)^2}$$

$$\theta_\perp = \frac{T_{\perp e}}{T_{\perp i}} \qquad \theta_\| = \frac{T_{\|e}}{T_{\|i}} \qquad \beta_\perp = \beta_{\perp i} + \beta_{\perp e}$$

Remark:

$$\gamma = \frac{2}{\sqrt{\pi}}\frac{T_{\|i}}{T_{\perp i}}\frac{|k_z|v_{th\|i}}{D} \times$$
$$\left\{\frac{T_{\perp i}}{T_{\|i}}\frac{C}{2} - (1+\theta_\perp)\left[1 + \frac{1}{\beta_\perp} + \frac{1}{\beta_\perp}\left(1 + \frac{\beta_\perp - \beta_\|}{2}\right)\frac{k_z^2}{k_\perp^2}\right]\right.$$
$$\left. -\frac{3}{4}\left(\frac{T_{\perp i}}{T_{\|i}} - 1\right)(1+B)k_\perp^2 r_L^2\right\}.$$

When the ion temperature anisotropy is small, the instability is not confined at large transverse scales. In this case, the functions $\Gamma_0(b_r)$ and $\Gamma_1(b_r)$ cannot be expended.

Examples of mirror instability extending to small scales

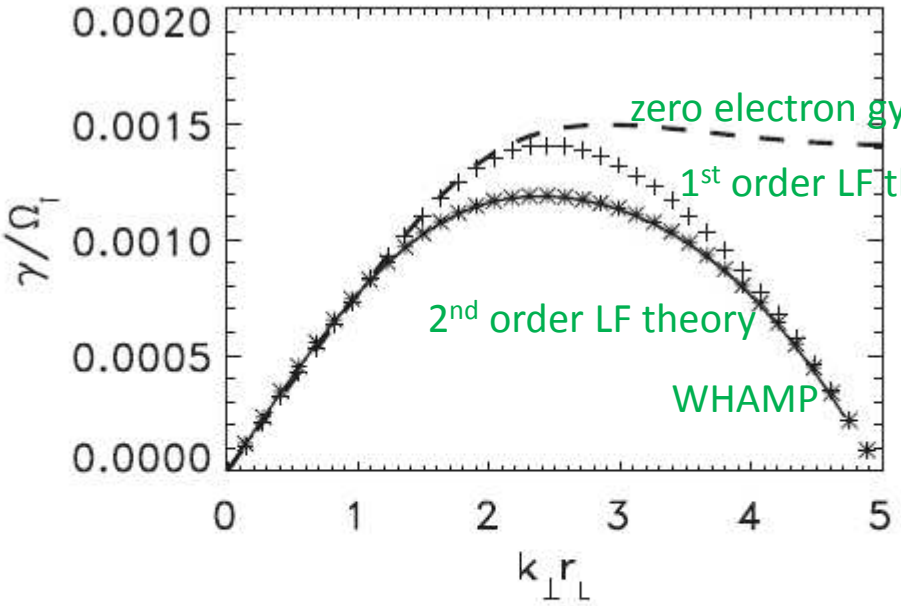

LF= low frequency

FIG. 1. Growth rate γ/Ω_i as a function of $k_\perp r_L$ for $\theta = 89°$, $\beta_{\|i} = 10$, $T_{\|e} = T_{\|i}$, $T_{\perp i}/T_{\|i} = T_{\perp e}/T_{\|e} = 1.094$ for the solution of WHAMP (solid line), the low-frequency theory using first-order (crosses) or second-order (stars) expansion, and from the first-order low frequency theory in the limit of zero electron gyro-radius (dashed line).

Example where the **ion response function is to be expended to second order** $R(\zeta_r) = 1 + i\sqrt{\pi}\xi_r - 2\zeta_r^2 + O(\zeta_r^3)$ and **electron FLR corrections must be retained**.

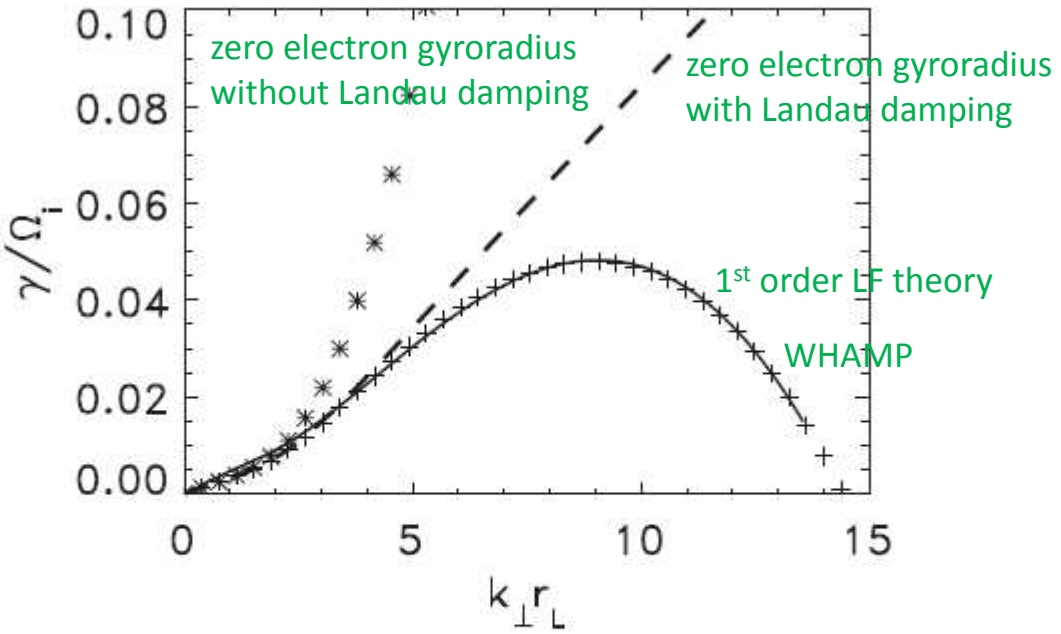

FIG. 2. Growth rate γ/Ω_i versus $k_\perp r_L$ for $\theta = 89°$, $\beta_{\|i} = 1$, $T_{\|e} = T_{\|i}$, $T_{\perp i}/T_{\|i} = 1.8$, $T_{\perp e}/T_{\|e} = 1.72$ from WHAMP (solid line), the first-order low-frequency theory (crosses), and the limit of zero electron gyro-radius with (dashed line) or without (stars) electron Landau damping.

Example where **Landau damping and FLR corrections are to be retained for the electrons.**

Nonlinear mirror modes

The nonlinear dynamics of mirror modes is a delicate issue.

Development of **mirror structures**: magnetic holes or humps, anti-correlated with density.

Magnetic humps
(or peaks)

Magnetic holes
(or dips)

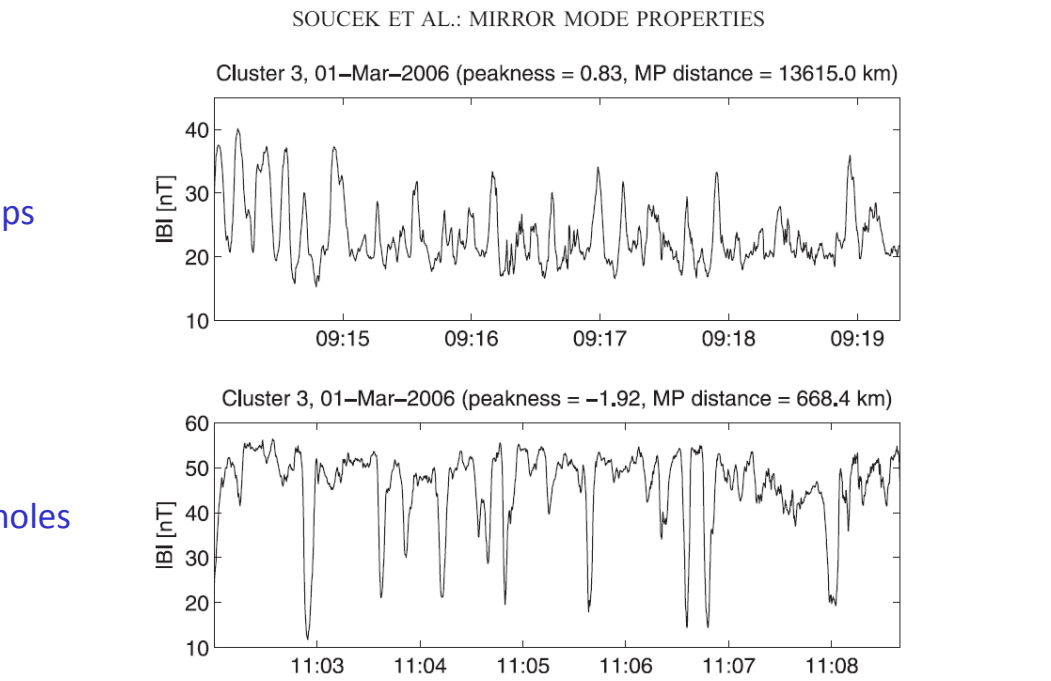

Figure 1. An example of mirror mode structures of the two types. (top) Peaks (peakness = 0.83), (bottom) dips (peakness = −1.92).

*Soucek et al., JGR **113**, A04203, 2007*

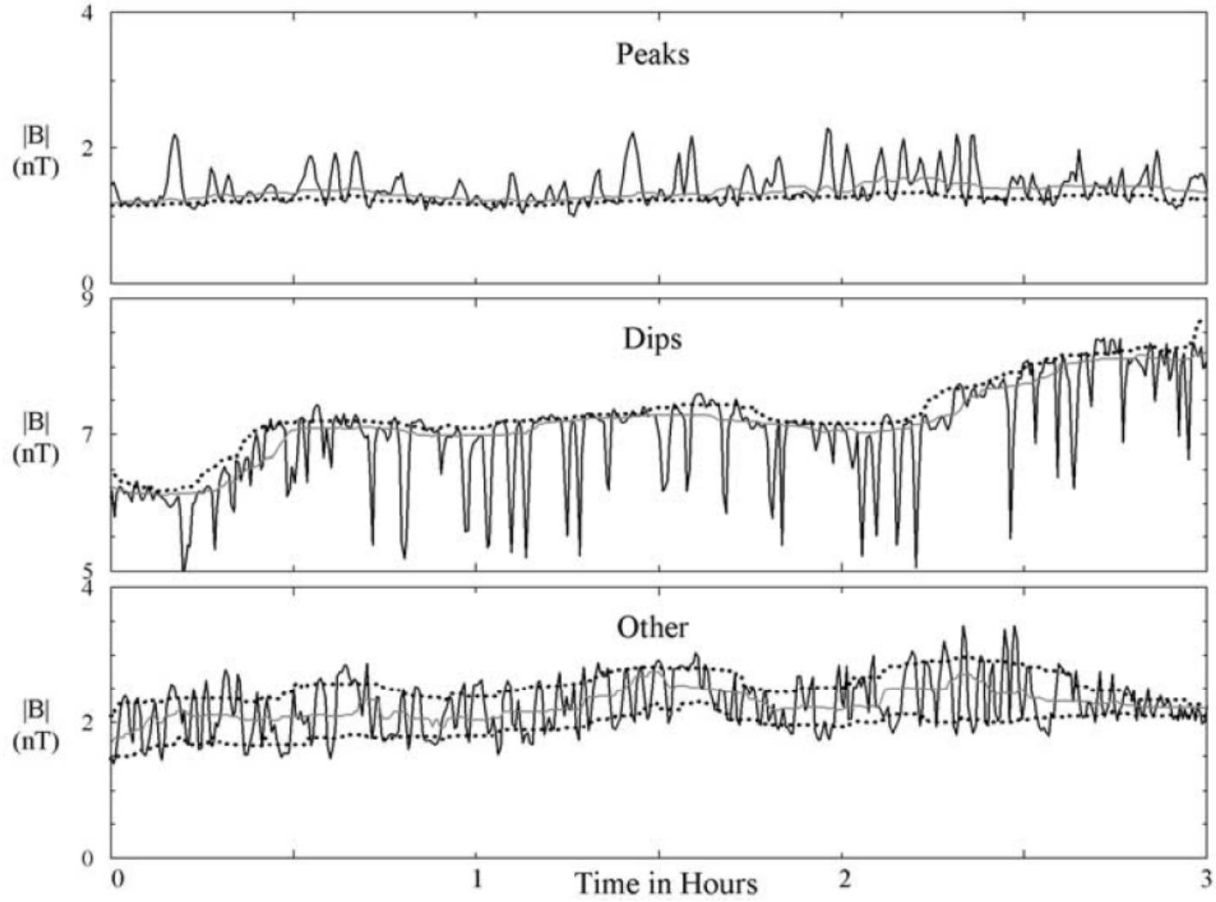

Figure 1. Each panel shows 3 hours of Galileo magnetometer field magnitude data (solid black line), appropriate quartiles (dotted), and the median value (solid gray) computed using 20 min sliding windows with single sample shifts. The panels show examples of "peaks" (top), "dips" (middle), and "other" (bottom) structures.

*Joy et al., GRL **111**, A12212 (2006)*

nearly sinusoidal modes

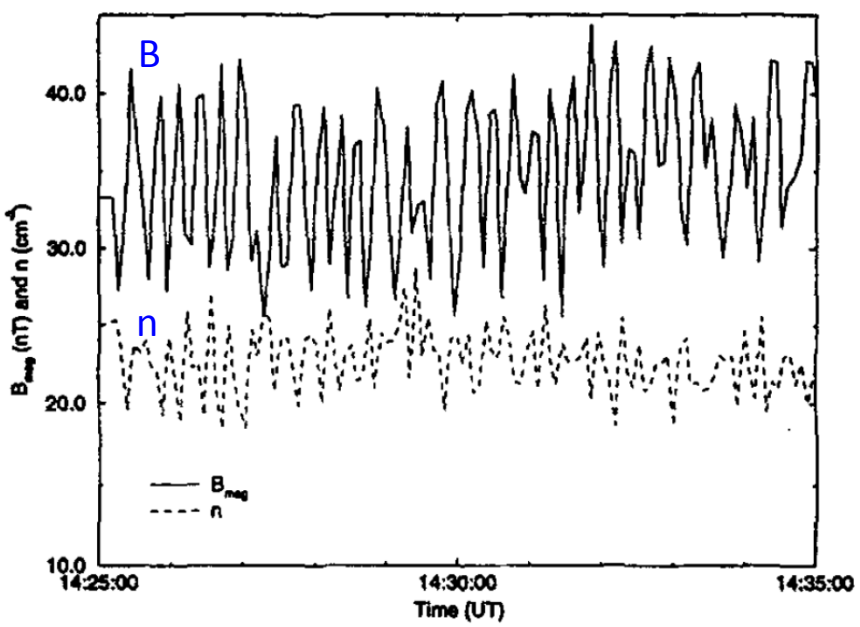

magnetic humps

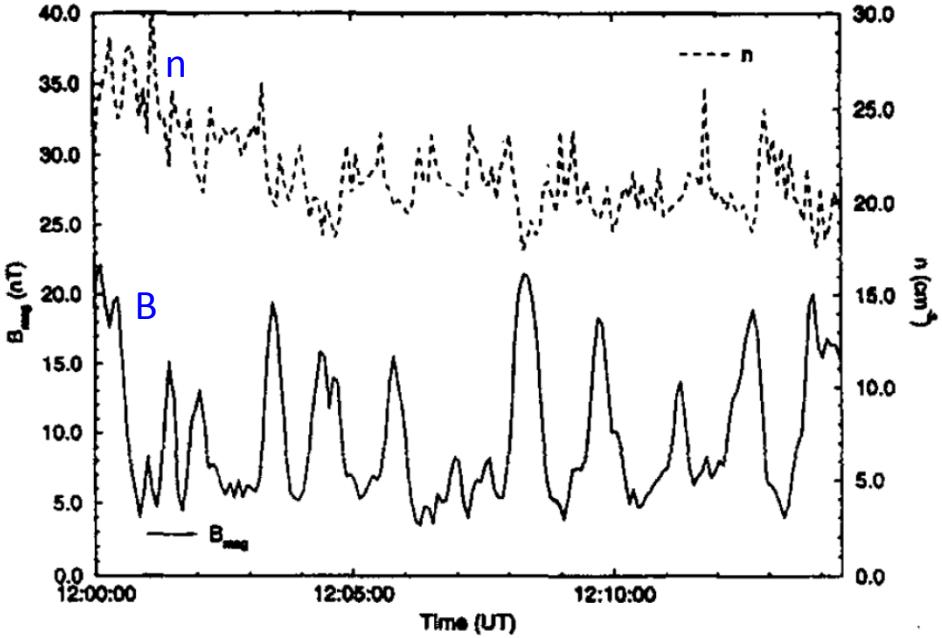

Strong anti-correlation of magnetic field and density for mirror modes.

Leckband et al., Adv. Space Res. ***15****, 345 (1995)*

Measurement by AMPTE-UKS satellite in the magnetosheath.

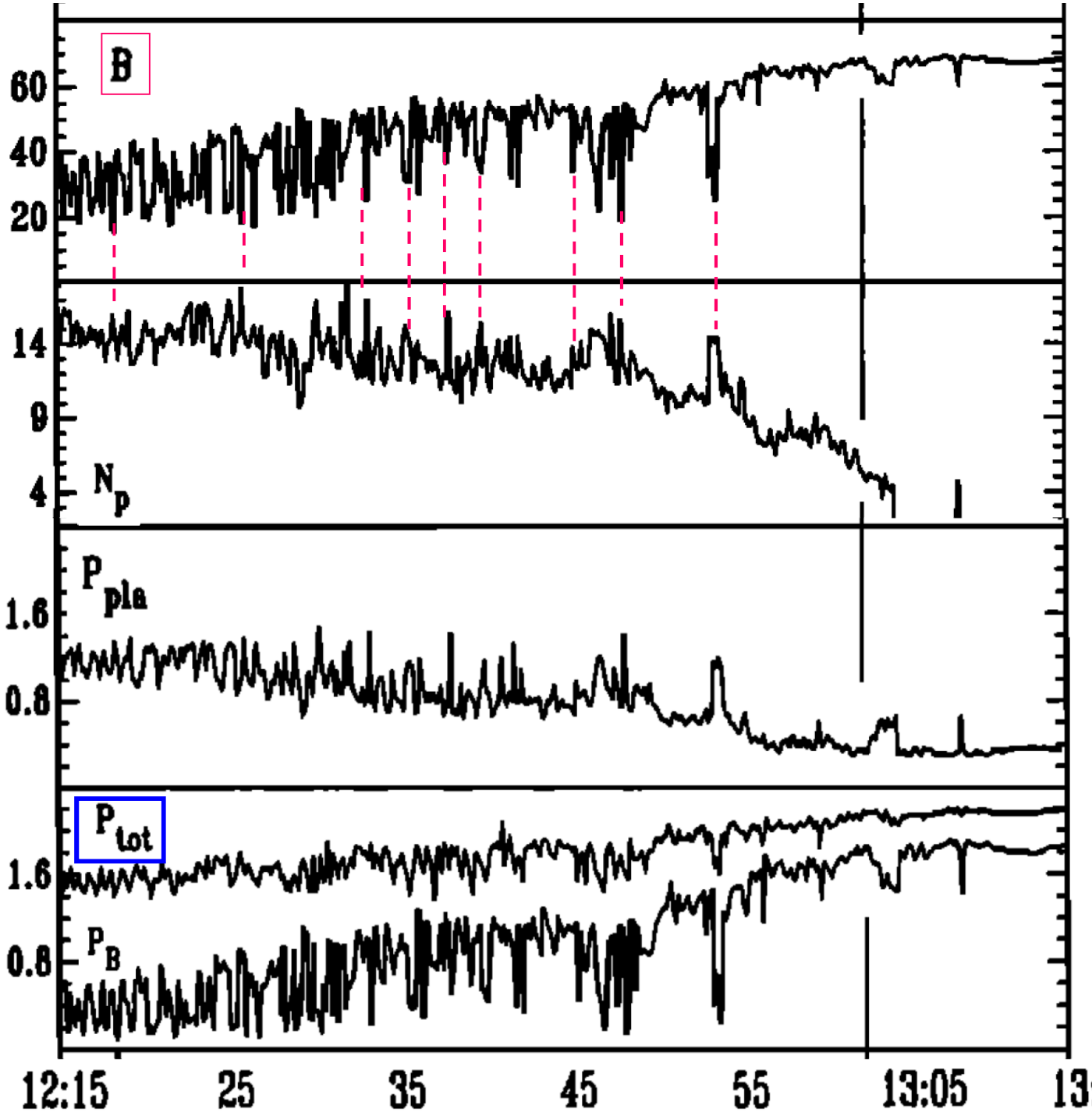

magnetic holes

anticorrelation
magnetic field - density

magnetosheath region adjacent to the dayside magnetopause (AMPTE/IRM satellite).

pressure equilibrium

*Phan et al. JGR **99**, 121, (1994)*

Holes at small β

Peaks at higher β

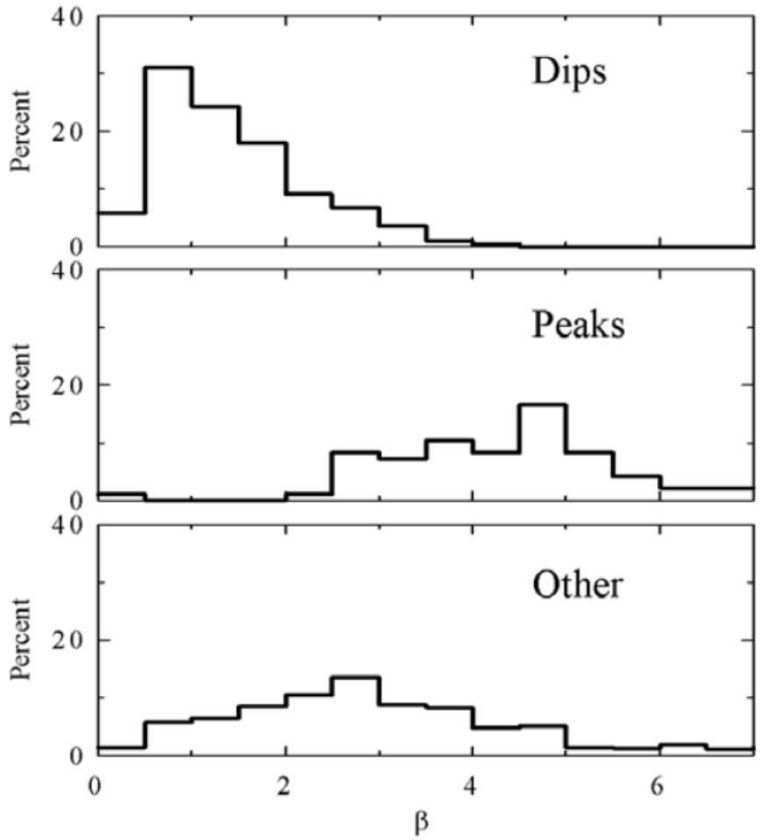

Figure 6. Occurrence distribution of MM structures versus plasma Beta (β).

*Joy et al., GRL **111**, A12212 (2006)*

A quantitative characterization of the shape of the mirror structures is provided by the *skewness* of the magnetic fluctuations *(Génot et al., Ann. Geophys.* ***27****, 601,2009)* or by the essentially equivalent *peakness* (defined as the skewness of the time series representing the total wavelet content betwen two chosen scales, of the original magnetic field fluctuations*) (Soucek et al.,* ***113****, A04203, 2007)*

Typically, a positive skewness corresponds to peaks
a negative skewness corresponds to holes

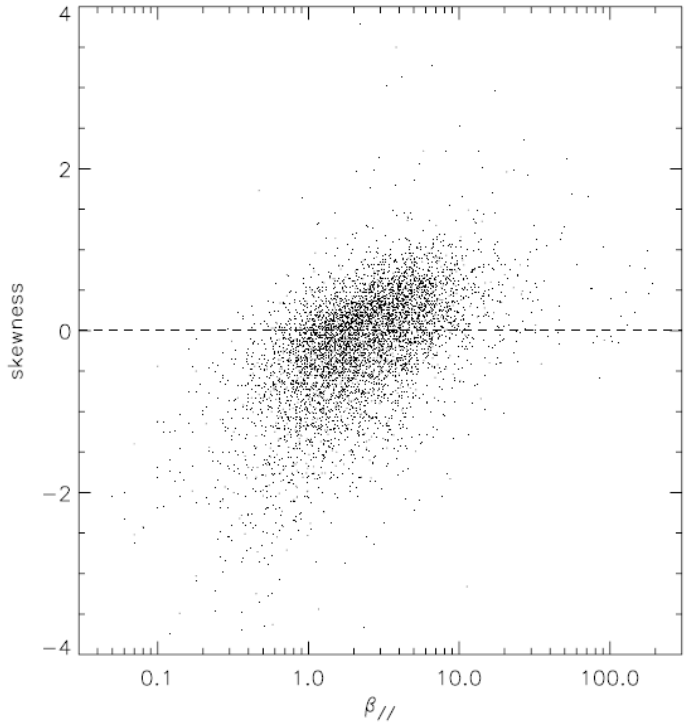

Fig. 3. Skewness as a function of $\beta_{\|}$ for all mirror events detected in the period 1 February 2001–31 December 2005.

Génot et al., Ann. Geophys. ***27****, 601 (2009)*

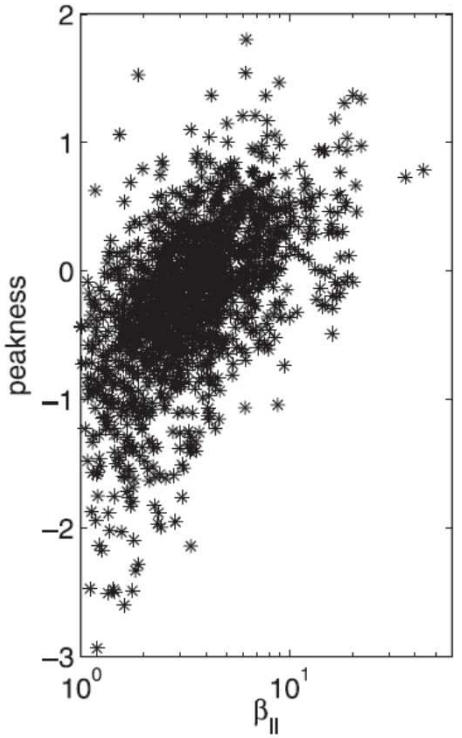

Soucek, JGR ***113****, A04203 (2007)*

Skewness variation with β

Influence of the distance to threshold

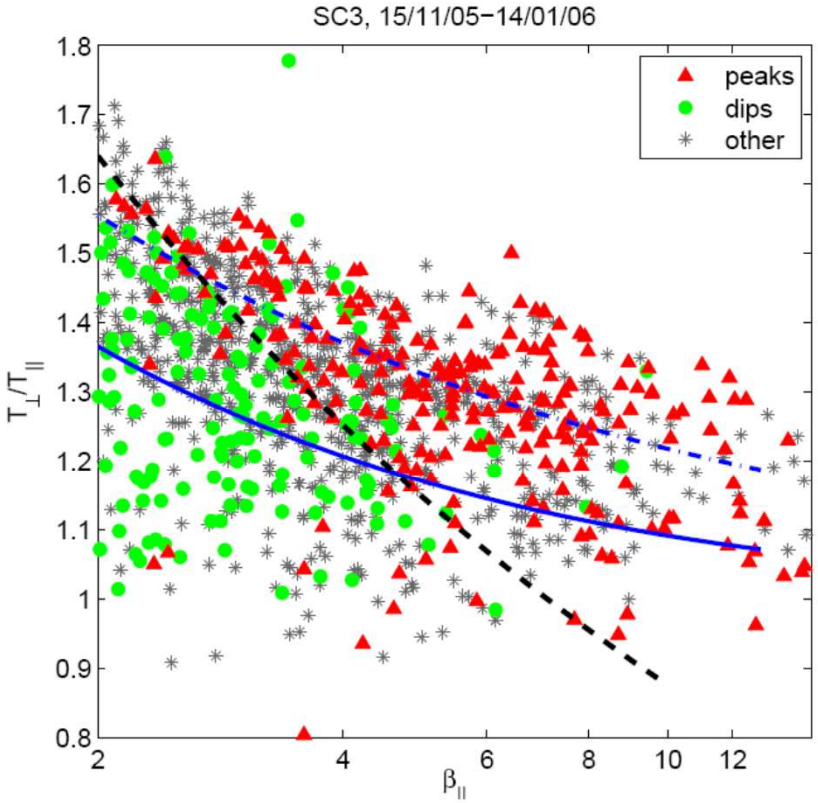

Figure 3. Distribution of mirror modes of different types in the anisotropy-beta plane. Red triangles denote peaks with $\mathcal{P} > 0.3$, green squares dips ($\mathcal{P} < -0.6$) and the remaining ambiguous mirror mode events are marked by grey stars.

Solid blue line: theoretical (bi-Maxwellian) mirror threshold

$$\frac{T_\perp}{T_{||}} > 1 + 1/\beta_\perp$$

Dashed-dotted blue line: empirical marginal stability

$$\frac{T_\perp}{T_{||}} = 1 + \frac{a}{\beta_{||}^b} \qquad a = 0.83 \quad b = 0.58$$

Black dashed line: fitted boundary between peaks and dips

$$\frac{T_\perp}{T_{||}} = \frac{2.15}{\beta_{||}^{0.39}}$$

"Peaks are typically observed in an unstable plasma, while **mirror structures observed deep within the stable region appear almost exclusively as dips".**

*Soucek, Lucek & Dandouras, JGR **113**, A04203 (2008)*

Solar wind: almost always stable against the mirror instability *(Winterhalter et al., Space Sc. Rev. **72**, 201, 1995)*: "Ulysses observed structures generated by mirror mode instability, which remained after the distribution relaxes to a marginally stable state".

"Although the plasma surrounding the holes was generally stable against the mirror instability, there are indications that the holes may have been remnants of mirror mode structures created upstream of the points of observation".

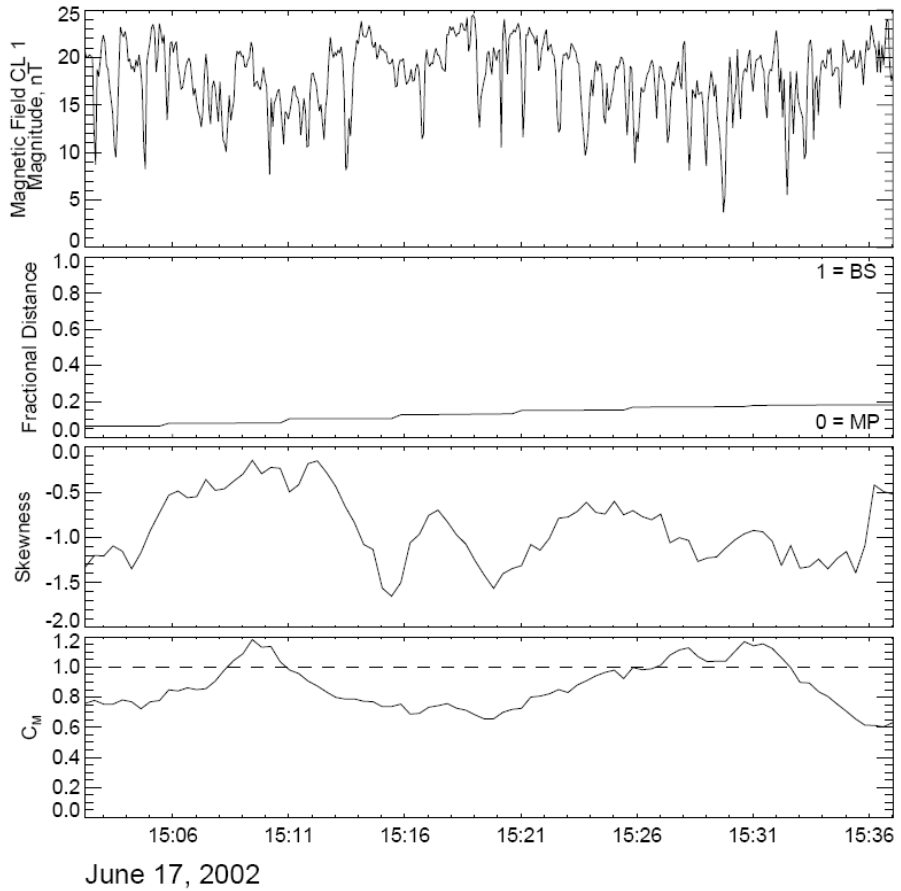

June 17, 2002

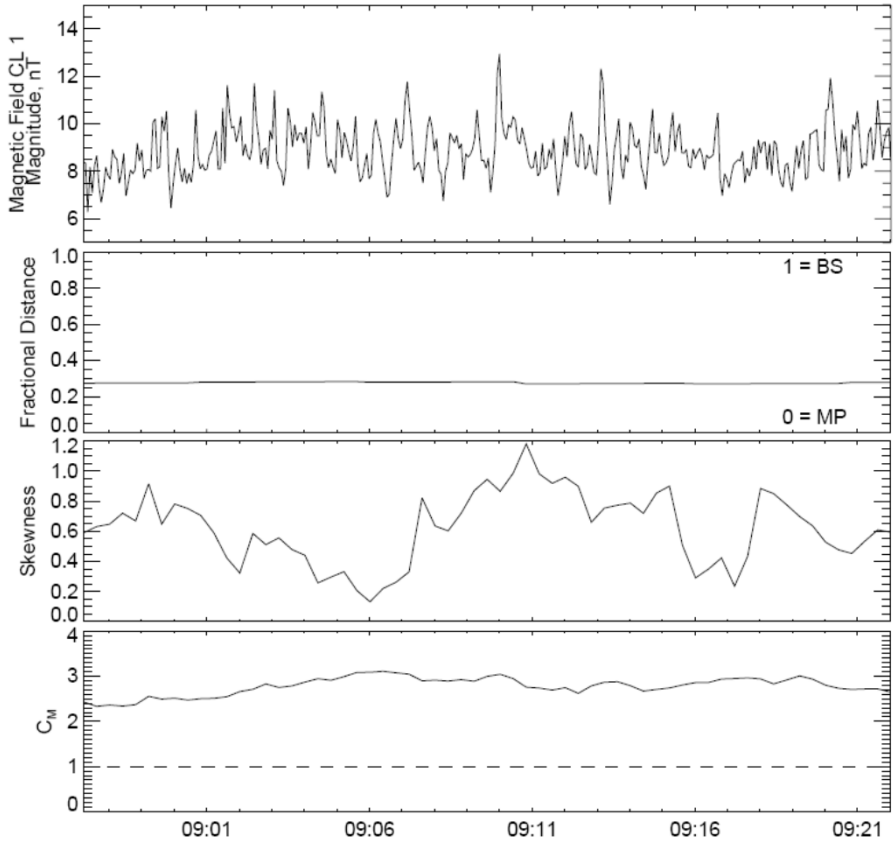

May 27, 2005

Magnetic **holes**
(Negative skewness)
Mostly subcritical

Magnetic **humps**
(Positive skewness)
Supercritical

$$C_M = \beta_{i\perp}\left(\frac{T_{i\perp}}{T_{i\parallel}} - 1\right).$$

$C_M - 1$ is then the distance to threshold.

C_M <1 : subcritical
C_M >1 : supercritical
(for cold electrons and bi-Maxwellian ions)

Génot et al., Ann. Geophys. ***27****, 601 (2009)*

(An estimate based on cold electrons and bi-Maxwellian ions is sufficient, given the data accuracy).

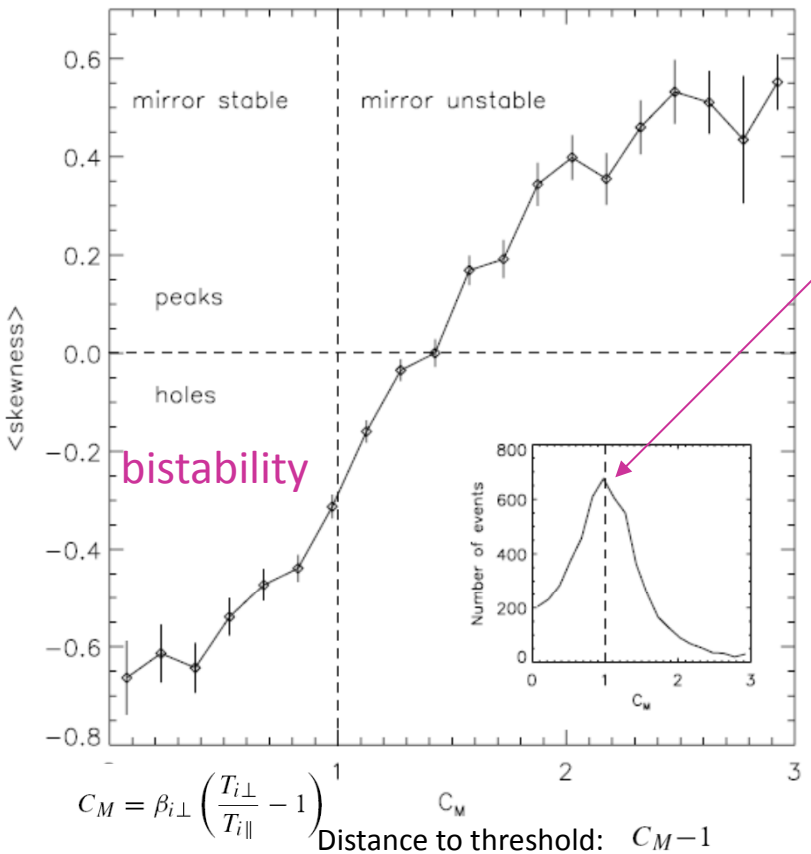

Fig. 5. Average skewness as a function of the mirror parameter C_M. The vertical dashed line delineates the mirror threshold. The horizontal dashed line delineates the region of predominance of holes (below) from the one of peaks (above). The error bars are proportional to $\sigma/\sqrt{N}$ where σ is the standard deviation and N is the number of mirror events in each ΔC_M=0.15 bin ($N_{\min}$=20 and $N_{\max}$=675). The insert shows the distribution of mirror events as a function of C_M: the peak is observed for marginally stable conditions with respect to the mirror instability ($C_M \simeq 1$).

Génot el al. 2009

Shows the tendency of the magnetosheath plasma to be mostly observed in a marginally stable state with respect to the mirror instability.

Peaks are a minority among mirror structures:

Joy et al. 2006: 14% are peaks; 19% holes

Soucek et al:2007: 18.7% are peaks; 39.7% holes

Holes are preferentially observed close to the magnetopause.

Peaks are more frequent in the middle magnetosheath.

Similar conclusions in *Soucek et al., 2007*

Consistent with *Bavassano Cattaneo et al. (1998).*

Magnetic peaks are only observed when the plasma is mirror unstable.

When the plasma is mirror stable, only magnetic holes are observed.

Numerical simulations of the Vlasov-Maxwell equations

*Califano, Hellinger, Kuznetsov, Passot, Sulem & Travnicek, JGR **113**, A012898, 2008*

Mirror unstable regime near threshold in a small domain (Eulerian scheme)

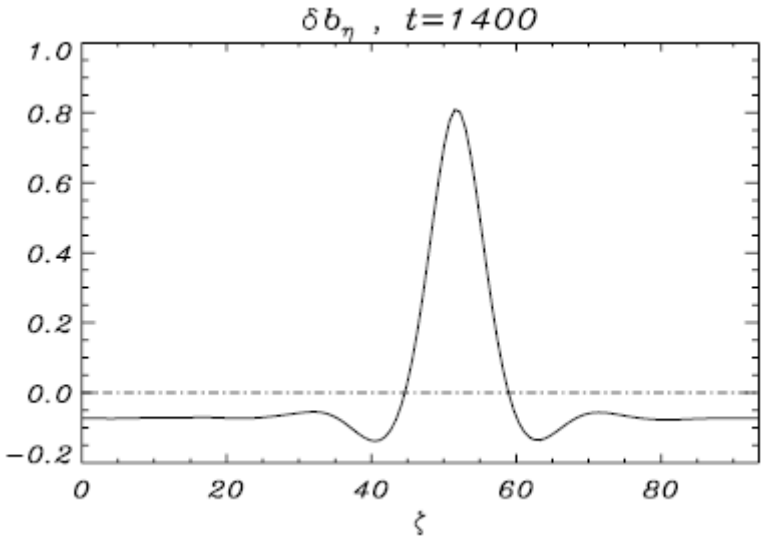

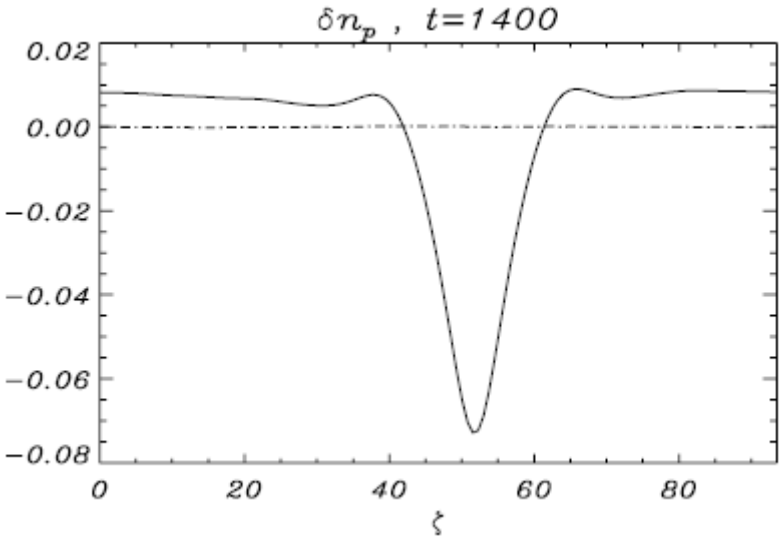

Figure 8. Magnetic and density fluctuation profiles at initial and final times of the simulation, in the case $T_\perp/T_\parallel = 1.4$, $\beta_\parallel = 15$ and $\theta = 78.53°$.

The mirror instability leads to the formation of magnetic peaks (and density holes).

Mirror unstable regime near threshold in an extended domain (PIC simulations)

1D simulation: $\theta_{kB} = 72.8°$ (most unstable direction)

$$\beta_{p\parallel} = 1 \; \beta_{p\perp} = 1.857 \qquad \beta_e = 10^{-2}$$

With a PIC code in a large domain:
Domain size= 2048 c/ω_{pi}
Growth rate: 0.005 Ω_p
1024 cells with 500 000

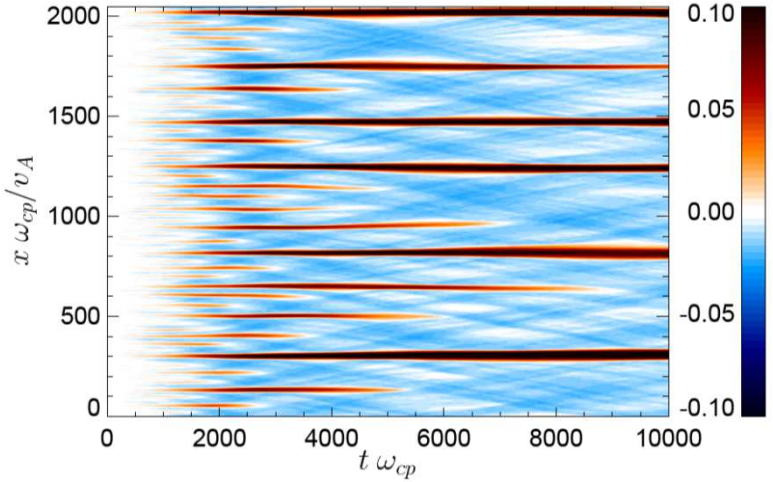

Color plot of the fluctuations of the magnetic field component B_η perpendicular to the direction ζ of spatial variation, as a function of ζ and t.

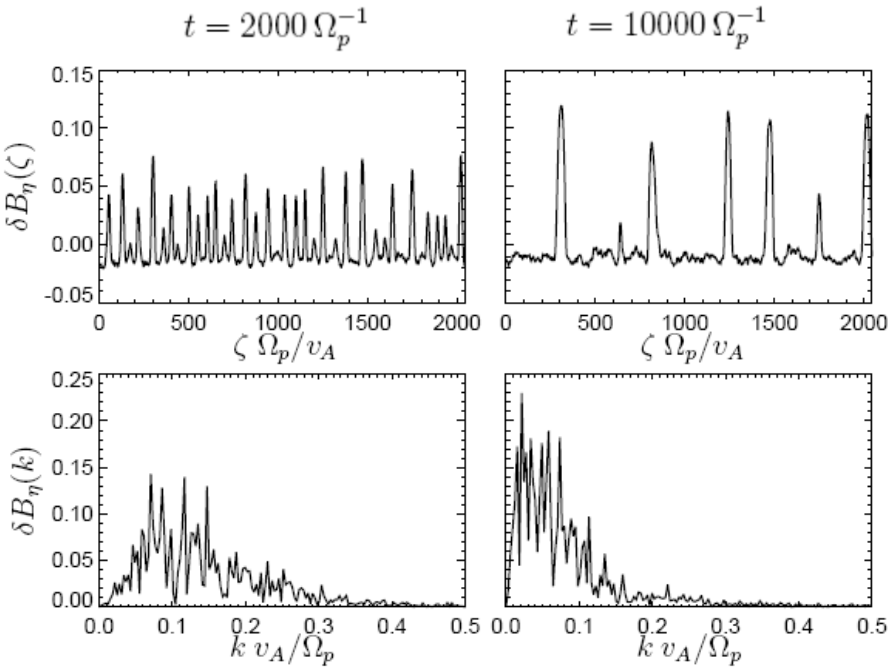

A large number of modes are excited.
Humps form and undergo coarsening.

Gray scale plot of the magnetic fluctuations as a function of space and time.

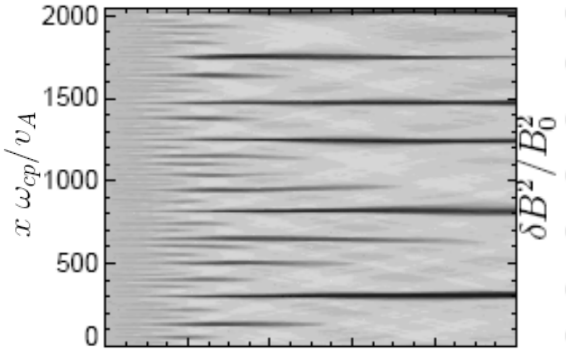

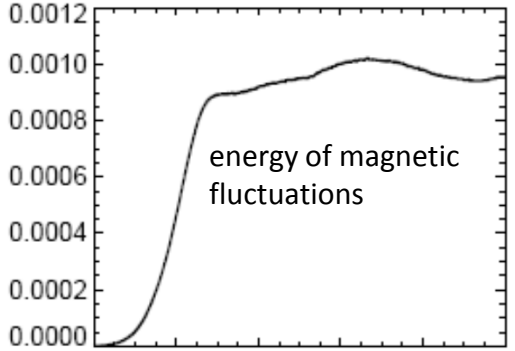

Bi-Maxwellian distance to threshold:

$$\Gamma^* = \beta_\perp \left(\frac{T_\perp}{T_\parallel} - 1 \right) - 1$$

Instantaneous distance to threshold:

$$\Gamma = -\frac{m_p}{p_B} \int \frac{v_\perp^4}{4} \frac{\partial f^{(0)}}{\partial v_\parallel^2} d^3v - \beta_\perp - 1$$

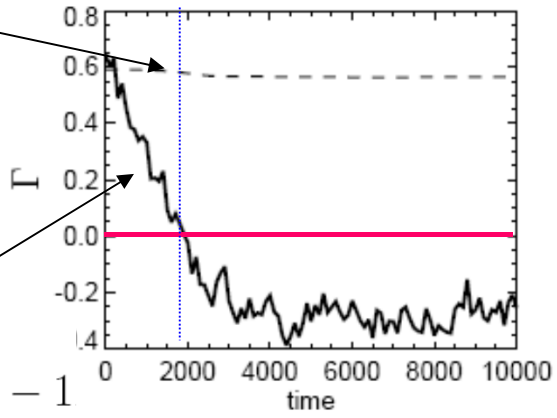

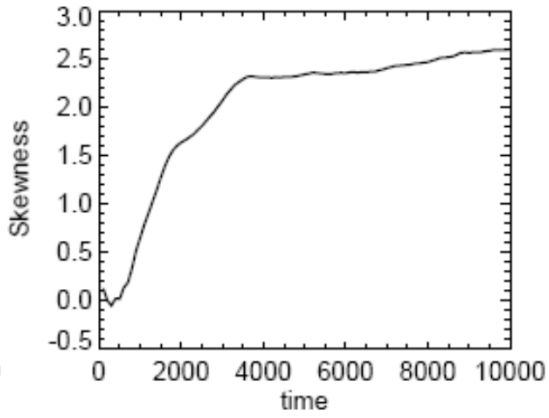

The actual distance to threshold rapidly departs from the bi-Maxwellian value, indicating a significant evolution of the proton distribution function.

Distance to threshold reaches negative values. No relaxation to marginal stability.

The instability continues to develop while Γ<0, due to the nonlinearities.
Positive skewness: magnetic humps.

Nonlinear development of the mirror instability leads to magnetic humps.

Toward a theoretical understanding of the nonlinear dynamics near threshold

A natural way to extend the linear theory to the weakly nonlinear regime (that develops near threshold), is to perform a reductive perturbative expansion based on the observation that, near threshold, the unstable modes are localized at large scale.

*Kuznetsov, Passot & Sulem, PRL **98**, 23003 (2007)*
*Califano et al., JGR **113**, A08219 (2008)*

Definitions:

$$
\begin{aligned}
p_B &= \frac{B_0^2}{8\pi} \\
p_\perp^{(0)} &= \frac{mn}{2}\int v_\perp^2 f^{(0)} d^3v \\
p_\Gamma &= -mn\int \frac{v_\perp^4}{4}\partial_{v_\parallel^2} f^{(0)} d^3v \\
\beta_\Gamma &= \frac{p_\Gamma}{p_B} \\
p_\Lambda &= \frac{mn}{8}\int v_\perp^6 \partial_{v_\parallel^2}^2 f^{(0)} d^3v \\
\beta_\Lambda &= \frac{p_\Lambda}{p_B} \\
\Gamma &= \frac{p_\Gamma - p_\perp}{p_B} - 1 = \beta_\Gamma - \beta_\perp - 1 \\
\Lambda &= \beta_\Lambda - 2\beta_\Gamma + \frac{\beta_\perp}{2} + \frac{1}{2} \\
\tilde{v}^{-1} &= -\sqrt{2\pi}\frac{mn}{p_B}\int \frac{v_\perp^4}{4}\delta(v_\parallel)\frac{\partial f}{\partial v_\parallel^2} d^3v \\
\tilde{r}^2 &= -\frac{mn}{24 p_B}\frac{1}{\Omega^2}\int\left(v_\perp^6\frac{\partial f}{\partial v_\parallel^2} + 3v_\perp^4 f\right) d^3v \\
\chi &= 1 + \frac{\beta_\perp - \beta_\parallel}{2} \\
b &= \frac{b_z}{B_0}
\end{aligned}
$$

normalized parallel magnetic fluctuations

$$
\begin{aligned}
\beta_\perp &= mnv_{th\perp}^2/p_B \\
\beta_\parallel &= mnv_{th\parallel}^2/p_B \\
\beta_\Gamma &= \beta_\perp^2/\beta_\parallel \\
\beta_\Lambda &= 3/2\beta_\perp^3/\beta_\parallel^2
\end{aligned}
\qquad
\begin{aligned}
\tilde{v} &= v_{th\parallel}/\beta_\Gamma \\
\tilde{r} &= v_{th\perp}(\beta_\Gamma - \beta_\perp)^{1/2}/\Omega \\
\Gamma &= \beta_\perp(\beta_\perp/\beta_\parallel - 1) - 1 \ll 1
\end{aligned}
$$

r_L: Larmor radius

For an arbitrary ion distribution function

$\sigma = \mathrm{sgn}\Gamma$

Hellinger et al., GRL ***36****, L06103 (2009)*

$$\partial_T b = \sqrt{\frac{2}{\pi}}\tilde{v}\,(-\mathcal{H}\partial_Z)\left(\sigma|\Gamma|b + \frac{3}{2}\tilde{r}^2\Delta_\perp b - \chi\,(\Delta_\perp)^{-1}\partial_{ZZ} b - \Lambda b^2\right)$$

distance to threshold — ion Larmor radius

Nonlinear contribution does not involve FLR corrections and can thus be computed within the drift kinetic approximation:
Kuznetsov et al., PRL ***98****, 235003 (2007).*
Pokhotelov et al., JGR, ***113****, A04225 (2008).*

Linear growth rate:

$$\gamma_{\boldsymbol{k}} = \sqrt{\frac{2}{\pi}}|k_\parallel|\tilde{v}\left(\Gamma - \frac{3}{2}\tilde{r}^2 k_\perp^2 - \frac{k_\parallel^2}{k_\perp^2}\chi\right)$$

For a bi-Maxwellian equilibrium proton distribution

$$f^{(0)} = \frac{1}{(2\pi)^{3/2} v_{th\parallel} v_{th\perp}^2}\exp\left(-\frac{v_\parallel^2}{2v_{th\parallel}^2} - \frac{v_\perp^2}{2v_{th\perp}^2}\right)$$

$$
\begin{aligned}
\partial_T b = \sqrt{\frac{2}{\pi}} v_{th\parallel}\frac{\beta_\parallel}{\beta_\perp^2}\left(-\mathcal{H}\partial_Z\right)\Big\{\Big[\beta_\perp\left(\frac{\beta_\perp}{\beta_\parallel} - 1\right) - 1\Big] b \\
+ \frac{3}{2} r_L^2 \Delta_\perp b - \left(1 + \frac{\beta_\perp - \beta_\parallel}{2}\right)\Delta_\perp^{-1}\partial_{ZZ} b - \frac{3}{2}\left(\frac{1+\beta_\perp}{\beta_\perp^2}\right) b^2\Big\}
\end{aligned}
$$

Califano et al. JGR ***113****, A08219 (2008)*

In the bi-Maxwellian case, $\Lambda > 0$

Defining

$$\xi = \sqrt{\frac{2}{3}}\frac{|\Gamma|}{\sqrt{\chi}}\frac{Z}{\tilde{r}} \qquad \tau = \sqrt{\frac{2}{\pi}}\frac{\Gamma^2}{\sqrt{\chi}}\frac{\tilde{v}T}{\tilde{r}}$$

$$\boldsymbol{R}'_\perp = \sqrt{\frac{2}{3}}\sqrt{|\Gamma|}\frac{\boldsymbol{R}_\perp}{\tilde{r}} \qquad u = \frac{|\Lambda|}{3|\Gamma|}b$$

σ=1: above threshold
σ =-1: below threshold

$$\partial_\tau u = (-\mathcal{H}\partial_\xi)(\sigma u + \Delta_\perp u - \Delta_\perp^{-1}\partial_{\xi\xi}u - 3\,\mathrm{sgn}(\Lambda)\,u^2)$$

Changing sign(Λ) replaces *u* by –*u*, indicating that
sign(Λ) prescribes the formation of peaks or holes.

For a bi-Maxwellian distribution, sgn(Λ) =1.

Case where spatial variations are limited to a direction making a fixed angle with the ambient field:

After a simple rescaling: $\partial_T U = \widehat{K}_\Xi\left[(\sigma + \partial_{\Xi\Xi})\,U - 3U^2\right]$

$\hat{K}_Z = -\mathcal{H}\,\partial_Z$
whose Fourier transform is $|K_Z|$

where Ξ is the coordinate along the direction of variation.

Bi-Maxwellian dynamics

When spatial variations limited to a direction making a fixed angle with the propagation:

$$\frac{\partial U}{\partial T} = \widehat{K}_{\Xi}\left[\left(\sigma + \frac{\partial^2}{\partial \Xi^2}\right) U - 3U^2\right]$$

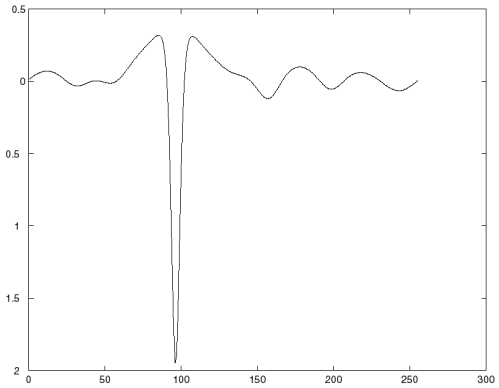

Profile of the solution near collapse

Integration above threshold (σ>1), with as initial conditions a sine function involving several wavelengths.

After an early phase of linear instability, **formation of magnetic holes,** whose number is progressively reduced to one.

The equation develops a finite time singularity with a self-similar behavior.

Wave-particle resonance provides the trigger mechanism leading to the linear instability.

Hydrodynamic nonlinearities reinforce the instability, leading to collapse.

Linear FLR effects arrest the linear instability at small scales but cannot cope with hydrodynamic nonlinearities.

At the level of Vlasov-Maxwell equations, the singularity is the signature of the formation of **finite-amplitude structures**, through a **subcritical bifurcation**.

*Kuznetsov et al., PRL **98**, 235003, (2007);*
*JETP Letters **86**, 637 (2007)*

A model possibly closer to numerical observations

Formation of magnetic hump could result from a distortion of the distribution function that does not remain close to bi-Maxwellian.

PIC simulation in an extended domain near threshold

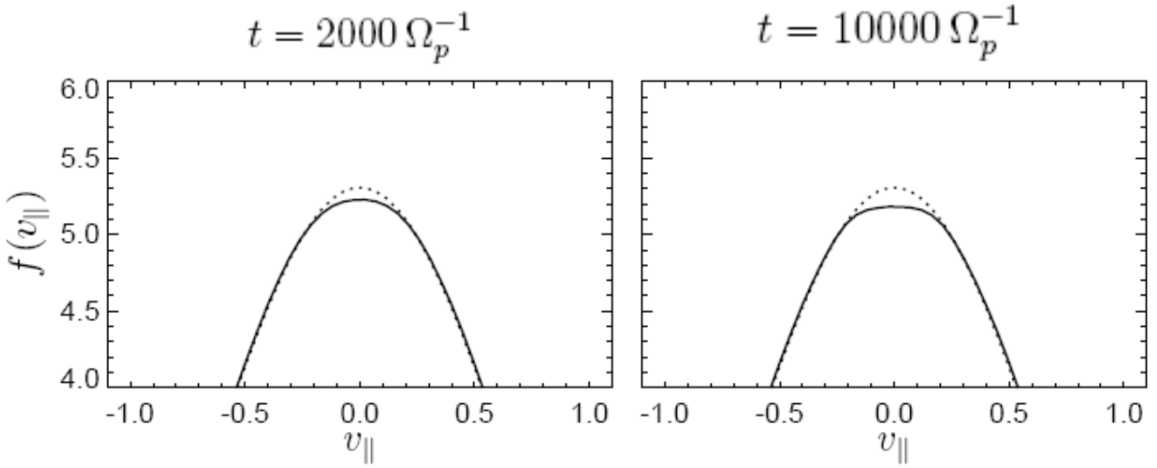

Reduced distribution function f as a function of $v_\parallel$ (solid curve) compared to the initial reduced distribution function (dotted curve).

Flattening of the distribution function

resulting from diffusion in velocity space

possibly described by the quasi-linear theory

Quasi-linear *theory* *(Shapiro & Shevchenko JETP **18**, 1109, 1963)*

- Assumes space homogeneity (thus no coherent structures); can thus be valid at early times only.
- Requires many modes in interaction, thus an extended domain.
- Can be extended to the (aperiodic) mirror instability because $\gamma_{\mathbf{k}} \ll k_z v_{th\,\|}$
- Describes a diffusion process in velocity space (dominantly along the ambient field).

Sketch of the method:

Ion distribution function: $f = f_0(t, \mathbf{v}) + f_1(t, \mathbf{r}, \mathbf{v})$

$$f_0(\mathbf{v}, t) = \langle f(\mathbf{x}, \mathbf{v}, t) \rangle_{\mathbf{x}}$$

$$\partial_t f + (\mathbf{v} \cdot \boldsymbol{\nabla}) f + \frac{q}{m}(\mathbf{E} + \frac{1}{c}\mathbf{v} \times \mathbf{B}) \cdot \boldsymbol{\nabla}_v f = 0$$

$$f_1 = \tfrac{1}{2} \sum_{\mathbf{k}} f_{\mathbf{k}}\, e^{i\mathbf{k}\mathbf{r}} + \text{c.c.}$$

$$\mathbf{E} = \tfrac{1}{2} \sum_{\mathbf{k}} \mathbf{E}_{\mathbf{k}}\, e^{i\mathbf{k}\mathbf{r}} + \text{c.c.}$$

$$\frac{1}{c}\partial_t \mathbf{B} = -\nabla \times \mathbf{E} \qquad \mathbf{B}_{\mathbf{k}} = -\frac{c}{\omega_{\mathbf{k}}} \mathbf{k} \times \mathbf{E}_{\mathbf{k}}$$

$$\partial_t f_0 = -\frac{q}{2m} \sum_{\mathbf{k}} \left\{ \mathbf{E}^*_{\mathbf{k}} \left(1 - \frac{\mathbf{k} \cdot \mathbf{v}}{\omega^*_{\mathbf{k}}} \right) + \frac{\mathbf{k}}{\omega^*_{\mathbf{k}}} (\mathbf{v} \cdot \mathbf{E}^*_{\mathbf{k}}) \right\} \nabla_{\mathbf{v}} f_{\mathbf{k}} + \text{c.c.}$$

Assumptions:

1. Variations of f_0 are slow compared with the variations of the fluctuations
2. Interactions between the harmonics of the collective motions are neglected : $f_{\mathbf{k}} = \mathcal{L}(f_0)$

linear

After some algebra, one gets a diffusion equation in the velocity space

$$D_{|||} = v_\perp^4 \sum_{\boldsymbol{k}} \frac{|b_{\boldsymbol{k}}|^2}{4} \frac{\gamma_{\boldsymbol{k}} k_\parallel^2}{k_\parallel^2 v_\parallel^2 + \gamma_{\boldsymbol{k}}^2}$$

$$D_{\perp\parallel} = -2\frac{v_\parallel}{v_\perp} D_{|||}$$

$$D_{\perp\perp} = v_\perp^2 \sum_{\boldsymbol{k}} \gamma_{\boldsymbol{k}} \frac{|b_{\boldsymbol{k}}|^2}{4}$$

$$\frac{\partial f}{\partial t} = \frac{\partial}{\partial v_\parallel} D_{|||} \frac{\partial f}{\partial v_\parallel} + \frac{1}{v_\perp} \frac{\partial}{\partial v_\perp} v_\perp \left(D_{\perp\parallel} \frac{\partial f}{\partial v_\parallel} + D_{\perp\perp} \frac{\partial f}{\partial v_\perp} \right)$$

$$\frac{\partial b_{\boldsymbol{k}}}{\partial t} = \gamma_{\boldsymbol{k}} b_{\boldsymbol{k}}$$

$$b_{\boldsymbol{k}} = \delta B_z(\boldsymbol{k})/B_0$$

linear growth rate computed from the instantaneous PDF

This equation was solved numerically

Hellinger & al., GRL, 36, L06103, (2009)

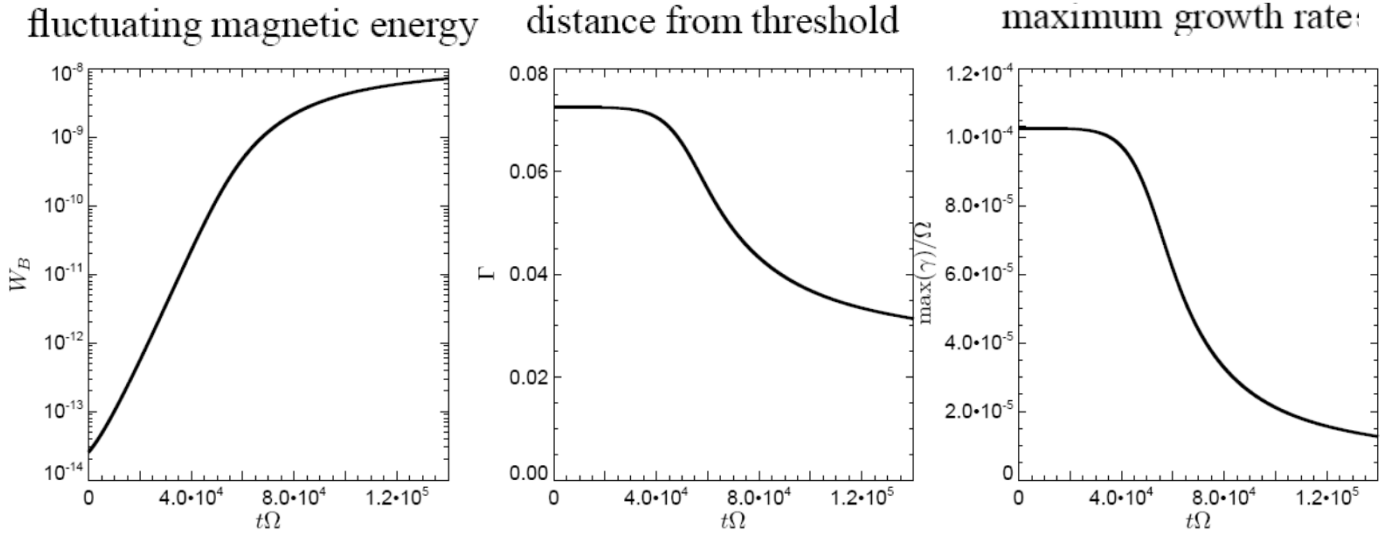

Quasi-linear theory cannot describe structure formation.
It traces the spatially independent part of the distribution function, while nonlinearities describing space variations (wave-wave interactions) are ignored.

Perturbation of the space-averaged distribution function $\Delta f = f - f^{(0)}$

QL theory

t= 1.4 10^5

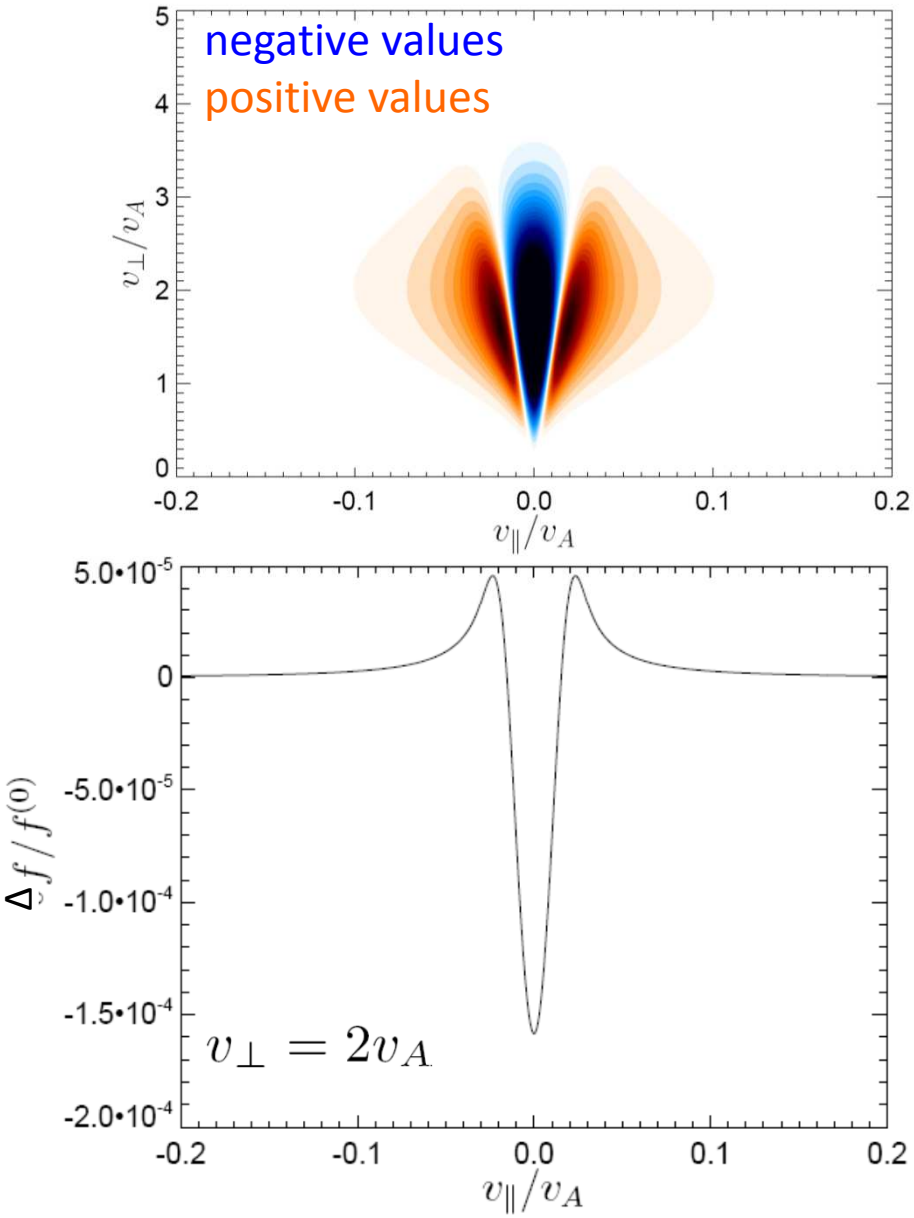

PIC simulation

t=2 10^3

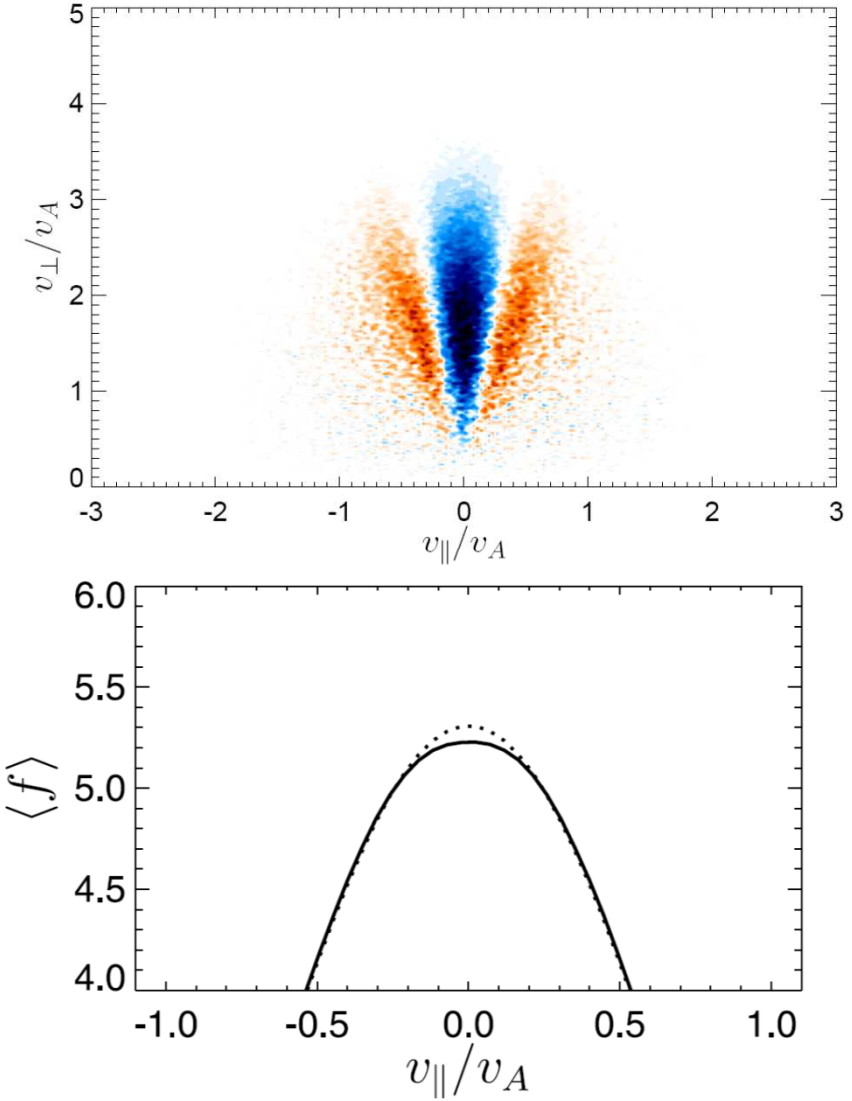

This suggests to couple QL theory and reductive perturbative expansion by estimating the coefficients in the equation for the magnetic fluctuations from the instantaneous QL distribution function (that is sensitive to the magnetic fluctuations).

$$\begin{cases} \dfrac{\partial f}{\partial t} = \dfrac{\partial}{\partial v_\parallel} D_{\parallel\parallel} \dfrac{\partial f}{\partial v_\parallel} + \dfrac{1}{v_\perp} \dfrac{\partial}{\partial v_\perp} v_\perp \left(D_{\perp\parallel} \dfrac{\partial f}{\partial v_\parallel} + D_{\perp\perp} \dfrac{\partial f}{\partial v_\perp} \right) \\ \\ \partial_t b = \dfrac{\sqrt{\frac{2}{\pi}}\tilde{v}}{1 + 2\frac{\tilde{v}}{v_\Lambda} b} \left(-\mathcal{H}\partial_z\right) \left(\Gamma b + \dfrac{3}{2}\tilde{r}^2 \Delta_\perp b - \chi \dfrac{\partial_z^2}{\Delta_\perp} b - \Lambda b^2 \right) \end{cases}$$

$b \equiv b_z$

$$v_\Lambda^{-1} = \sqrt{2\pi} \frac{mn}{p_B} \int \frac{v_\perp^6}{8} \delta(v_\parallel) \frac{\partial^2 f}{(\partial v_\parallel^2)^2} d^3v$$

Hellinger & al., GRL, 36, L06103, (2009)

The coupled system can also be viewed as retaining the full nonlinear equation for the magnetic fluctuations given by the reductive perturbative theory within the QL description, instead of the sole linear contribution.

Because of the quasi-singularity of the distribution function resulting from the QL evolution, near the zero parallel velocity, contributions of the resonant particles are to be taken into account when estimating the nonlinear coupling (**nonlinear Landau damping**), which leads to the **denominator**.

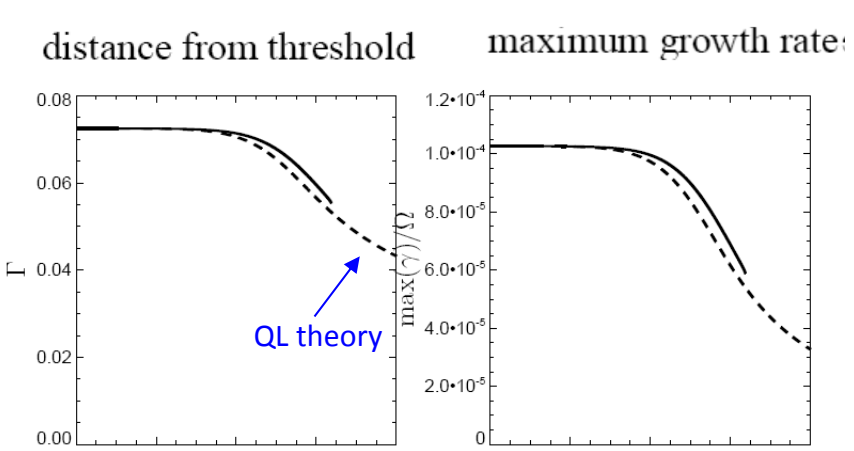

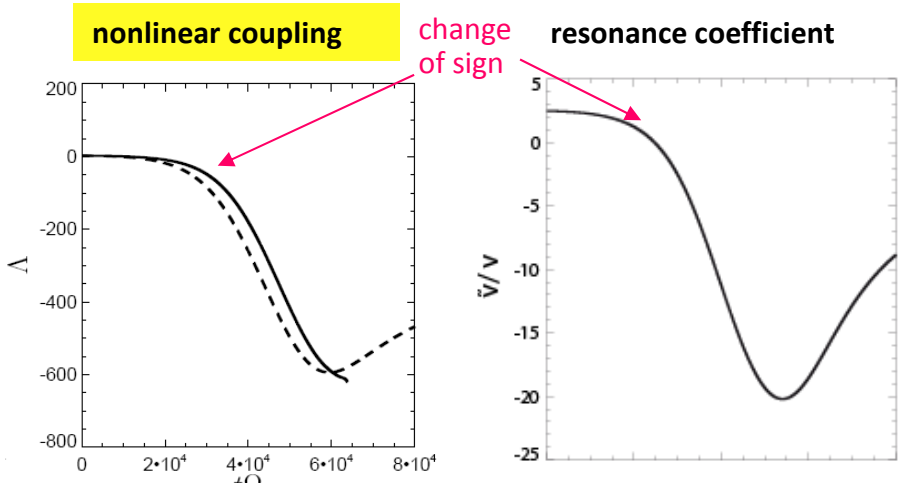

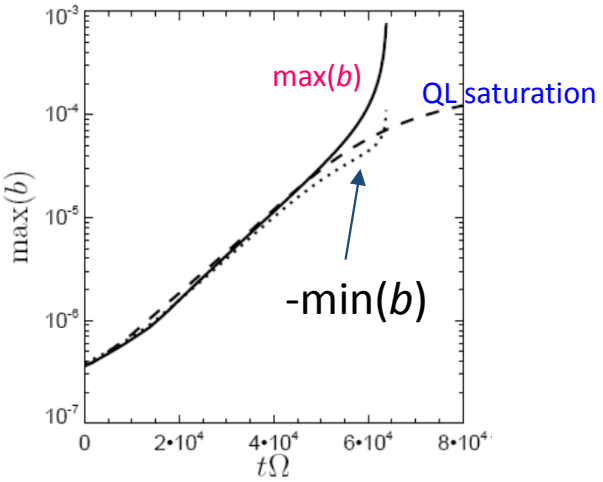

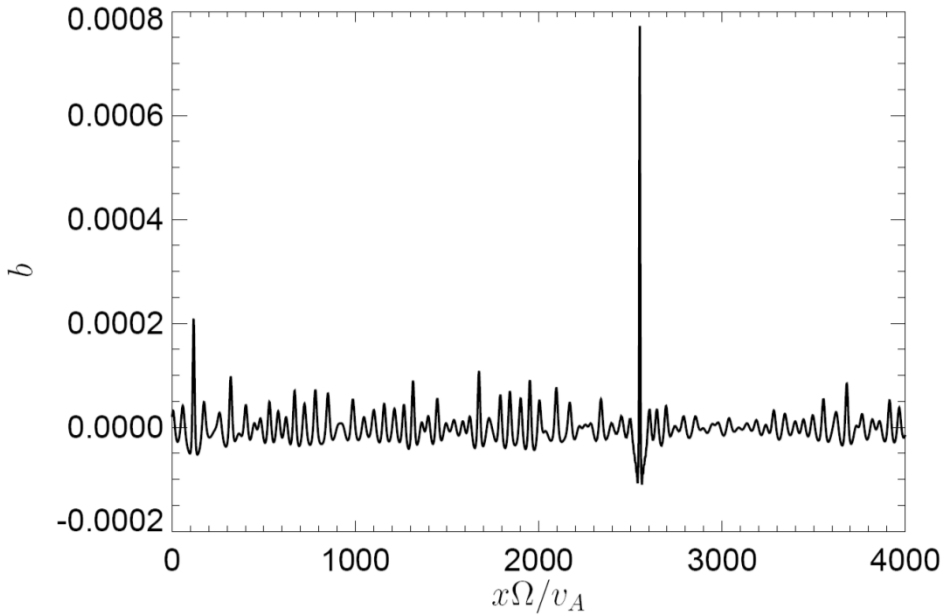

Formation of **magnetic humps**

Results of the simulation of coupled system in 1D (in the most unstable direction)

Saturation by nonlinear Landau damping

Difficult to study the saturation by direct integration of the model (due to numerical limitations).

In order to isolate the saturation effect, we freeze the coefficients after the QL phase
(QL diffusion is expected to be strongly depleted as structures are formed)

1D model after rescaling,

$$\partial_t b = \frac{1}{1+s\alpha b}\left(-\mathscr{H}\partial_\xi\right)\left(\sigma b + \mu\,\partial_{\xi\xi} b - 3sb^2\right)$$

where σ=+1 (supercritical) or -1 (subcritical)

s=+1 (near a Maxwellian distribution)

or s=-1 (due to QL flattening of the distribution function)

The parameters α and μ are positive.

The denominator is reminiscent (in a small amplitude expansion) of the *arctan* trapping correction suggested in *Pokhotelov et al., JGR **113**, A04225, 2008).* The physical mechanism is however different, originating here from nonlinear Landau damping.

The parameter α refers to the contribution of the QL resonance to the nonlinear coupling.

While for α=0, the solution blows up in a finite time, the **denominator arrests the collapse** at a maximal amplitude given by 1/α, leading to the formation of

- magnetic dark solitons when s=+1
- magnetic bright solitons when s=-1

*(Passot et al., AIP Conf. Proc. **1188**, 205, 2009)*

Saturated solutions in a supercritical regime

Numerical integration of the model equation, starting from a sine wave of amplitude 0.01 in a domain of size 2π leads to a stationary hump.

The problem is numerically delicate: Extremely small time steps are required.

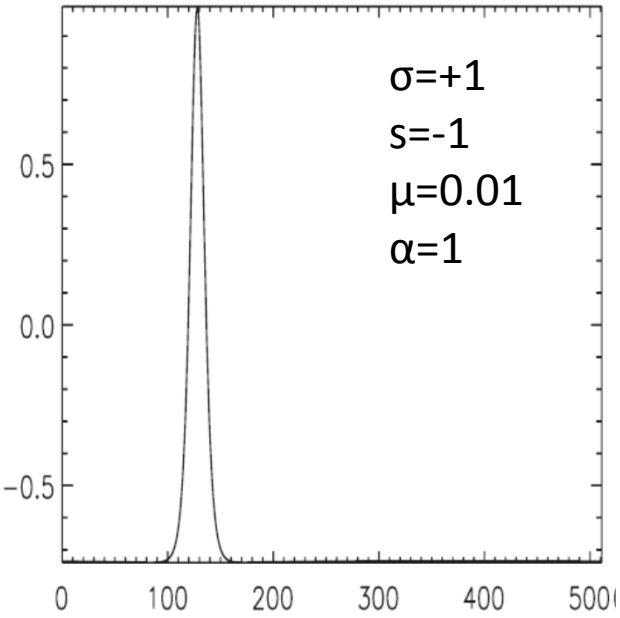

Saturation process:

During the nonlinear phase of amplitude growth, a plateau of negative values gradually develops, that tends to locally reduce the ambient magnetic field, putting the system in a situation similar to the subcritical regime.

The solution is thus attracted to the KdV soliton with an amplitude $b_{max}=1/\alpha$: Amplitude is prescribed by the strength of the early time QL resonance: larger amplitudes when these effects are weaker.

When starting with random initial conditions, which leads to a large number of humps, a coarsening phenomenon is observed.

When QL effects are subdominant (even above threshold), s=+1 and hole solutions are obtained (change b into –b).

Subcritical solutions

When σ=-1 with large initial data, no quasi-linear phase: the distribution function remains bi-Maxwellian (s=+1).

The denominator correction (with α small) is to be retained because of the large amplitudes.

Magnetic holes are obtained.

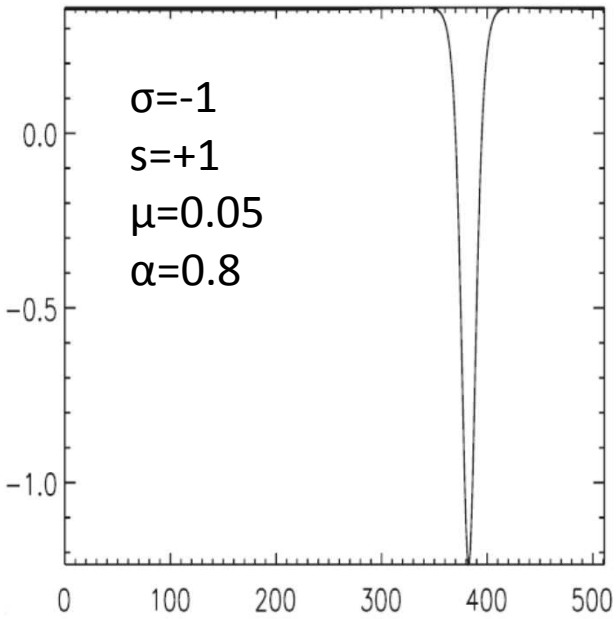

Mirror instability far from threshold

PICS simulations

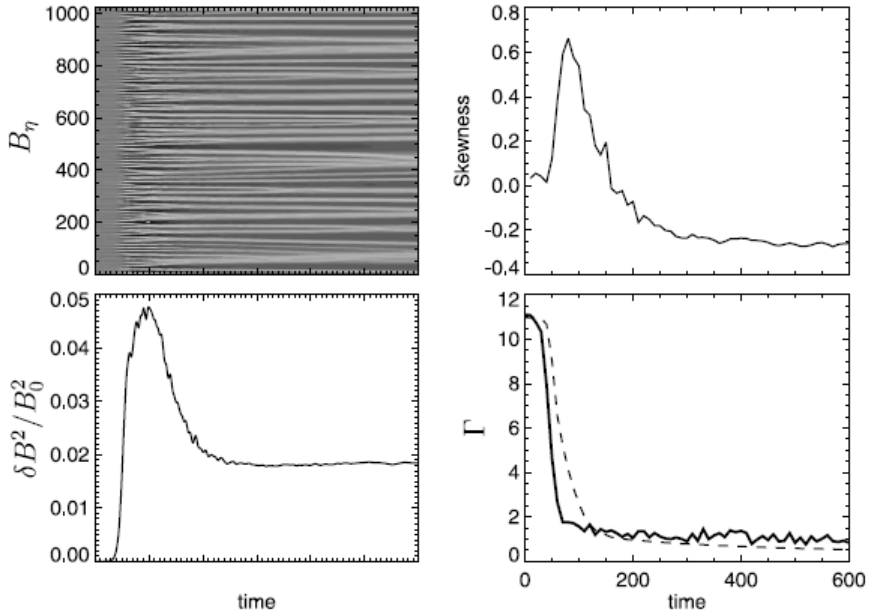

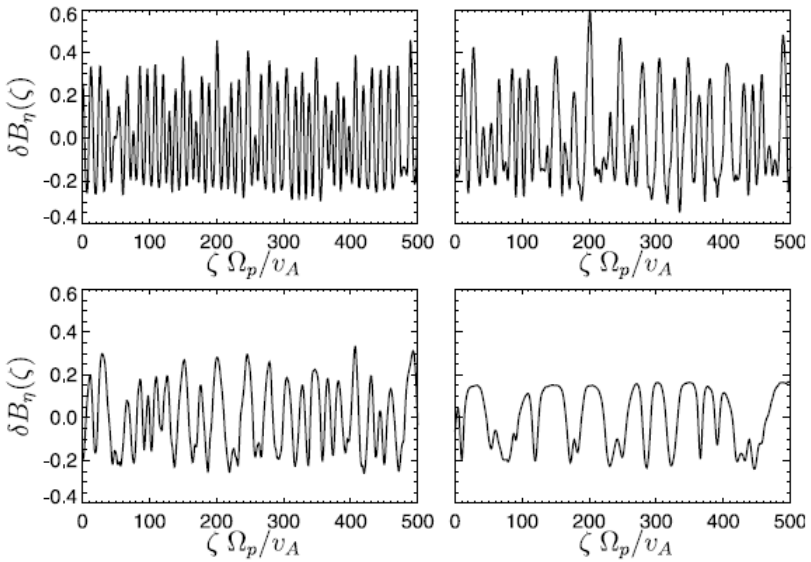

Figure 16. Evolution in an extended domain, for $\beta_\parallel = 1$, $T_\perp/T_\parallel = 4$ and $\theta = 50.5°$. Gray scale plot of the magnetic fluctuation B_η as a function of time and space (left top); Time evolution of skewness of B_η (right top), of fluctuating magnetic energy $\delta B^2/B_0^2$ (left bottom), of the instantaneous distance from the threshold (right bottom): Γ (solid line) as given by equation (1) and the corresponding bi-Maxwellian value Γ^* (dashed line) obtained from equation (2).

Figure 17. Profiles of δB_η as a function of ζ in a fraction of the simulation box, in the conditions of Figure 16. From left to right and top to bottom: $t = 60/\Omega_p$, $t = 100/\Omega_p$, $t = 150/\Omega_p$, and $t = 600/\Omega_p$.

Transition from magnetic peaks to magnetic holes during the time evolution

*Califano et al., JGR **113**, A012898, 2008*

STEREO observations on the solar wind

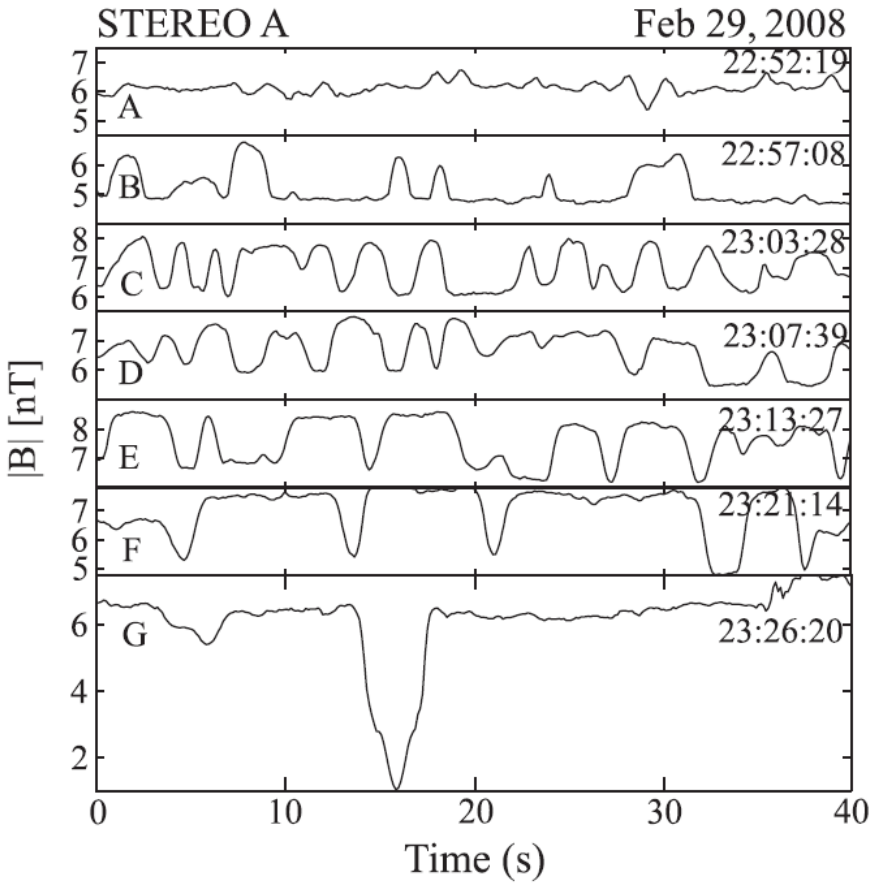

Figure 4. Forty seconds segments of *B* showing the development of magnetic structures during mirror mode storms observed on 29 February 2008. The starting time (HH:MM:SS) of each segment is indicated on the right hand side.

Figure 4 shows the evolution of the mirror-mode structures in intervals of 40 s during the storm. At the very beginning of the event, near the shock, mirror-mode waves are mainly small amplitude "peaks" (top of Figure 4A). A few minutes later, the number of peaks increases, and the time separation between them decreases (Figures 4B–4C). As time passes, holes begin to be detected, making it difficult to distinguish between peaks and holes (Figure 4D). Near the end of the storm event, the structures turn into nicely shaped holes which are deeper, wider, and more separated as the end of the event is approached (Figures 4F–4G). The normalized amplitudes ($\delta B/B_0$) of such holes can reach $\delta B/B_0 = 0.95$ approximately as seen in the hole presented in case G of Figure 4. During the MMS, the mean value of beta was 11.48 with a maximum peak of 51.59.

*Enriquez-Riviera et al. JGR **118**, 1, 2013*

Summary

In a non-collisional (or weakly collisional plasma), the ion pressure is usually non isotropic (significantly weaker collisions may be sufficient to make electron temperature isotropic).

At large enough scales, the pressure tensor is gyrotropic,.
At small scales , finite Larmor radius effects induce non-gyrotropic contributions.

Pressure (or temperature) anisotropy may be due to the expansion/compression of the plasma and to other processes such as turbulence which induce (anisotropic) heating or cooling.

Anisotropic heating may lead to **microinstabilities** that constrain the development of the anisotropy, maintaining the system close to the instability threshold.

Mirror instability is one of the processes leading to magnetic holes and humps commonly observed in heliospheric plasmas.

Temperature anisotropy can also play a role in other contexts (not addressed here), such as an effect on the growth rate of the tearing instability in magnetic reconnection
(Matteini et al. ApJ , in press).